The United Nations University

GEOTHERMAL TRAINING PROGRAMME
Orkustofnun, Grensásvegur 9,
IS-108 Reykjavík, Iceland

Reports 2002
Number 2

HYDROTHERMAL MINERAL BUFFERS CONTROLLING REACTIVE GASES CONCENTRATION IN THE GREATER OLKARIA GEOTHERMAL SYSTEM, KENYA

M.Sc. Thesis
Department of Geology and Geography,
University of Iceland

by

Cyrus W. Karingithi
Kenya Electricity Generating Co., Ltd.
Olkaria Geothermal Project
P.O. Box 785, Naivasha
KENYA

United Nations University,
Geothermal Training Programme
Reykjavík, Iceland
Report 2 - 2002
Published in September 2002

ISBN 9979-68-099-7

This M.Sc. thesis has also been published in September 2002 by the
Department of Geology and Geography,
University of Iceland

INTRODUCTION

This document is a MSc thesis submitted to the department of Geology and Geography in the University of Iceland (Háskóli Íslands). The study entailed sampling and analysis of separated water, steam and rock cuttings taken from high temperature geothermal wells in the Greater Olkaria geothermal area, Kenya. The state of equilibrium between the reactive gases and selected hydrothermal mineral buffers in the Olkaria geothermal system was evaluated. The study was supervised by Professor Stefán Arnórsson of the Science Institute, University of Iceland.

The study started in May 2000, with the six months geothermal training course at the United Nations University at Orkustofnun, sampling and analysis in January - February 2001 and was completed in August 2002.

With warmest wishes from Iceland,

Ingvar B. Fridleifsson, director,
United Nations University
Geothermal Training Programme

ACKNOWLEDGEMENTS

Special thanks to my supervisor, Professor Stefán Arnórsson, I am truly honoured to have been his student. My sincere gratitude to the UNU Staff – Dr. Ingvar B. Friðleifsson, Mr. Lúdvík S. Georgsson and Mrs. Gudrún Bjarnadóttir, for their generous help, care and advice during the whole study period.

I would like to thank the UNU, the Government of Iceland, the University of Iceland (Háskóli Íslands), and the KenGen management for funding and providing any other assistance required for the study. Geology & Geography Department staff, Science Institute staff, Orkustofnun staff and the Nordic Volcanological Institute staff are sincerely thanked for all the assistance they gave.

My deepest thanks to my family for all the sacrifice they made during the study. This thesis is dedicated to them. All glory and honour to the Lord for the successful completion of the entire study.

ABSTRACT

The Greater Olkaria geothermal system in Kenya is located within the Olkaria central volcanic complex in the central sector of the Kenya Rift Valley, to the south of Lake Naivasha and 120 km from Nairobi, the capital city of Kenya. Olkaria is a high temperature geothermal system, with aquifer temperatures between 200 ˚C and 340 ˚C. A total of 102 deep wells have been drilled in the area, ranging in depth from 500 to 2800 m. Two power plants are presently in operation, with a total generating capacity of 57 MWe. A 64 MWe, power plant is under construction in Olkaria Northeast field.

The fluid chemistry of each individual field has been studied and characterised. Application of the Cl-SO_4-HCO_3 ternary diagram shows that wells in the Olkaria West field discharge sodium-bicarbonate type water, while wells in Olkaria East and Olkaria Northeast fields discharge alkaline sodium chloride type water. Olkaria Central and Olkaria Domes wells discharge a mixture of the sodium chloride and sodium bicarbonate end member fluid types (Karingithi, 2000). The total concentration of dissolved solids (TDS) in the fluid discharged by wells in the Greater Olkaria geothermal system is low, compared to most high-temperature geothermal systems in the world. The chloride concentration in the water at the weirbox varies between 100 and 1100 ppm, being lowest in well OW-304D and highest in well OW-10. The wells in Olkaria East and Olkaria Northeast tend to be highest in chloride. This could be the consequence of an up-flow of deep high-temperature geothermal fluid, although progressive boiling by heat flow from the rock may also contribute in the Olkaria East field well discharges.

The water at the weirbox is alkaline (pH 8.1 to 9.9 as measured at 20 ˚C) and is relatively high in bicarbonate, which ranges from 90 ppm in Olkaria East to 13,000 ppm in some of the wells in Olkaria West. The CO_2 concentration in the steam phase varies from 0.67 mmoles/mole of steam in well OW-30 in the Olkaria East field to 206.5 mmoles/mole of steam in well OW-304D located in Olkaria West field. The concentration of H_2S varies from 0.009 mmoles/mole of steam in well OW-902 in Olkaria Domes, to 0.168 mmoles/mole of steam in well OW-20 in the Olkaria East field. The H_2 concentration varies from 0.000 in well OW-202 in Olkaria Central field to 0.095 mmoles/mole of steam in well OW-23 in Olkaria East.

Twenty-six thin sections of rock cutting chips from eight high temperature geothermal wells in the Greater Olkaria geothermal area were prepared and the chemical composition of garnet and epidote measured. From the chemical composition of these minerals the average activity of grossular and clinozoisite of 0.43 and 0.07, respectively, were calculated.

Aquifer fluid compositions were calculated with the aid of the WATCH speciation programme (Arnórsson et al., 1982), version 2.1A, (Bjarnason, 1994). This code computes individual aqueous species activities in producing aquifers from analytical data on water and steam samples collected at the wellhead, as well as values for the activity products (Q) for the respective mineral reactions. To assess the state of

equilibrium between aqueous CO_2, H_2S, and H_2 concentrations in the Olkaria geothermal reservoir and selected hydrothermal mineral buffers, equilibrium constants (K) for selected mineral solute reactions were derived from thermodynamic data, taking into account the effects of variable mineral composition, as appropriate.

The equilibrium state of the aquifer water at Olkaria has been assessed for various end-member hydrothermal minerals, mineral pairs and mineral buffers found in the reservoir rock. The equilibrium constants (K) for mineral pairs/buffers controlling the $Ca^{+2}/(H^+)^2$ and $Fe(OH)_4^-/OH^-$ activity ratios were retrieved and the temperature dependence functions derived. The subsequent saturation indices were evaluated. The aquifer waters in the Olkaria geothermal reservoir are at equilibrium or very close to equilibrium with respect to the following minerals; calcite, clinozoisite, epidote, and prehnite. Evidence indicates that the aquifer waters are also close to equilibrium with respect to pyrite, pyrrhotite and magnetite. Thus the H_2S/H_2 activity ratio corresponds closely to equilibrium with the mineral pairs pyrite/pyrrhotite and pyrite/magnetite. However, the present results indicate general under-saturation with respect to the individual minerals. This apparent under-saturation is considered to be the consequence of faulty thermodynamic data on iron (Fe) hydrolysis constants.

The aquifer waters are moderately undersaturated with respect to grossular and wollastonite. The calcium/proton squared ($Ca^{+2}/(H^+)^2$) activity ratios of the aquifer waters are on average slightly lower than the equilibrium values for the mineral pair of grossular-clinozoisite but close to equilibrium value for the prehnite-clinozoisite. The aquifer waters have higher $Fe(OH)_4^-/OH^-$ activity ratios than the equilibrium values for the mineral pair epidote-prehnite and the mineral buffer epidote-wollastonite-grossular-quartz. This is probably due to the overestimation of the $Fe(OH)_4^-$ species. The aquifer fluid is at equilibrium with respect to the mineral pairs of pyrite/pyrrhotite and pyrite/magnetite, with respective saturation indices of 0.16 and 0.006. The activities of aqueous H_2 and H_2S gases generally correspond closely to equilibrium with the mineral buffer pyrite/pyrrhotite/magnetite. Samples showing low H_2 and H_2S values with respect to the equilibrium with the above buffer are from marginal wells whose discharge fluid is mixed with atmospherically contaminated fluid. The activities of aqueous H_2 and H_2S also correspond closely to equilibrium with the mineral buffer pyrrhotite-prehnite-epidote-pyrite. At present it is not possible to conclusively identify which of the two buffers control the activities of the aqueous H_2 and H_2S. The clinozoisite-calcite-quartz-prehnite buffer is considered to control the CO_2 activity in the aquifer.

TABLE OF CONTENTS

Page

1.0 INTRODUCTION 1

2.0 HISTORY OF GEOTHERMAL DEVELOPMENT 3

3.0 GEOLOGICAL FEATURES AND PHYSICAL RESERVOIR CHARACTERISTICS 5
3.1 Geology and stratigraphy 5
3.2 Hydrothermal minerals 7
3.3 Pressure and temperature 7
3.4 Well discharge enthalpy 9
3.5 Fluid compositions 9

4.0 SAMPLING AND ANALYSIS 11
4.1 Water samples 11
4.2 Electron microprobe analysis 11

5.0 CALCULATION OF AQUIFER FLUID COMPOSITION, AQUEOUS SPECIATION AND MINERAL-GAS EQUILIBRIUM CONSTANTS 13
5.1 Aquifer fluid composition computation 13
5.2 Aqueous speciation 14
5.3 Thermodynamics of minerals, aqueous species and mineral solubility constants 14
5.4 Errors in calculated mineral solubility constants 15

6.0 MINERAL BUFFERS CONTROLLING, REACTIVE GASES CONCENTRATION 16
6.1 Calcite 16
6.2 Clinozoisite and epidote 18
6.3 Prehnite 20
6.4 Grossular 21
6.5 Magnetite, pyrite and pyrrhotite 21
6.6 Wollastonite 27
6.7 Calcium ion / proton activity ratios 27
6.8 $Fe(OH)_4^-$ / OH^- activity ratios 30
6.9 Carbon dioxide 30
6.10 Hydrogen and hydrogen suplphide 32

7.0 SUMMARY AND CONCLUSIONS 37

REFERENCES 39

TABLES 45

LIST OF FIGURES

Page

1.1 Map of the Kenya rift faults showing major volcanoes and location of Olkaria 2
2.1 Geothermal fields within the Greater Olkaria geothermal area 3
3.1 Volcano-tectonic map of the Greater Olkaria geothermal area 5
3.2 E-W geological cross section 6
3.3 E-W temperature cross section 8
6.1 Aquifer temperature versus log Q 16
6.2 Aquifer pH versus calcite SI 17
6.3 Aquifer steam fraction versus aquifer pH for well OW-2 and OW-301 18
6.4 Aquifer temperature versus activity product (clinozoisite) 19
6.5 Aquifer temperature versus activity product (epidote) 19
6.6 Aquifer temperature versus activity product (prehnite) 20
6.7 Aquifer temperature versus activity product (grossular) 21
6.8 Aquifer pH versus grossular SI 22
6.9 Aquifer temperature versus activity product (pyrite) 22
6.10 Aquifer temperature versus activity product (pyrrhotite) 23
6.11 Aquifer temperature versus aquifer Fe^{+2} 24
6.12 Aquifer temperature versus (H_2S/H_2) activity ratio (pyrite – pyrrhotite) 24
6.13 Aquifer temperature versus activity product (magnetite) 25
6.14 Aquifer temperature versus H_2S/H_2 activity ratio (pyrite – magnetite) 26
6.15 Aquifer temperature versus log H_2S in aquifer water (pyrrhotite – pyrite – magnetite) 26
6.16 Aquifer temperature versus log H_2 in aquifer water (pyrrhotite – pyrite – magnetite) 27
6.17 Aquifer temperature versus $Ca^{+2}/(H^+)_2$ activity ratio (wollastonite) 28
6.18 Aquifer temperature versus $Ca^{+2}/(H^+)_2$ activity ratio (wollastonite – quartz) 28
6.19 Aquifer temperature versus log (a_{Ca+2} / a^2_{H+}) activity ratio (prehnite – clinozoisite) . . 29
6.20 Aquifer temperature versus log (a_{Ca+2}/a^2_{H+}) activity ratio
(grossular – clinozoisite – quartz) 29
6.21 Aquifer temperature versus log ($a_{Fe(OH)4-} / a_{OH-}$) activity ratio (epidote – prehnite) . . . 30
6.22 Aquifer temperature versus log ($a_{Fe(OH)4-} / a_{OH-}$) activity ratio
(epidote – wollastonite – quartz – grossular) 31
6.23 Aquifer temperature versus log CO_2 in aquifer water
(clinozoisite – calcite – quartz – prehnite) 31
6.24 Aquifer temperature versus log CO_2 activity ratio
(clinozoisite – calcite – quartz – grossular) 32
6.25 Aquifer temperature versus log H_2S in aquifer water
(pyrrhotite – pyrite – prehnite – epidote) 33
6.26 Aquifer temperature versus log H_2 in aquifer water
(pyrrhotite – prehnite – epidote – pyrite) 33
6.27 Aquifer temperature versus log H_2S in aquifer water
(grossular – pyrite – pyrrhotite – quartz – epidote – wollastonite) 34
6.28 Aquifer temperature versus log H_2 in aquifer water
(grossular - pyrrhotite – quartz – epidote – wollastonite – pyrite) 35
6.29 Aquifer temperature versus log H_2S in aquifer water
(grossular – magnetite – pyrite – quartz – epidote – wollastonite) 35
6.30 Aquifer temperature versus log H_2 in aquifer water
(grossular – magnetite – quartz – epidote – wollastonite) 36

LIST OF TABLES

Page

1. Chemical analysis results from selected Olkaria geothermal wells 45
2. Geothermal wells whose rock cuttings were selected for microprobe analysis 46
3. Epidote and Garnet solid solutions chemical formulae 47
4. Thermodynamic properties of selected secondary end-member minerals at Olkaria geothermal system 48
5. Temperature equations for the equilibrium constant for individual minerals reactions 49
6. Mineral pairs reactions controlling calcium/proton and hydrogen sulphide/hydrogen activity ratio in solution and respective log K temperature equations 50
7. Temperature equations for the equilibrium constant for selected mineral-gas buffers 51

1.0 INTRODUCTION

Recent studies have successfully demonstrated that the gas concentration in geothermal well discharges is controlled by temperature-dependent equilibria between alteration minerals in the reservoir rock and gas concentration or gas ratios in the producing aquifer (Arnórsson and Gunnlaugsson, 1985).

Studies of the state of hydrothermal mineral-solution equilibria are of importance for quantifying the chemical composition of fluids discharged from geothermal wells. Changes with time in the fluid compositions provide valuable information on the response of exploited reservoir to the production load, such as cold recharge and fluid quality. Many studies have demonstrated that geothermal water compositions are controlled by close approach to various mineral-solution equilibria with respect to all major elements except chloride, at least if the temperatures exceed 100°C and in some cases at lower temperatures (Giggenbach 1981; Arnórsson et al., 1983; Arnórsson and Andrésdóttir, 1995; Palandri and Reed, 2000; Stefánsson and Arnórsson 2000; Gudmundsson and Arnórsson, 2002).

The objective of the present study is to assess the state of equilibrium between aqueous CO_2, H_2S, and H_2 concentrations in the Olkaria geothermal reservoir and selected hydrothermal mineral buffers. The study involves two steps:

1) derivation of equilibrium constants (K) for selected mineral solute reactions from thermodynamic data, taking into account the effects of variable composition of the minerals, as appropriate, and
2) calculation of individual aqueous species activities in producing aquifers from analytical data on water and steam samples collected at the wellhead to retrieve values for the activity products (Q) for the respective reactions.

The Greater Olkaria geothermal system in Kenya is located within the Olkaria central volcanic complex in the central sector of the Kenya Rift Valley, to the south of Lake Naivasha and 120 km from Nairobi, the capital city of Kenya (Figure 1.1). Olkaria is a high temperature geothermal system, with aquifer temperatures between 200°C and 340°C. A total of 102 deep wells have been drilled in the area ranging in depth from 500 to 2800 m. Two power plants are presently in operation, with a total generating capacity of 57 MWe. A 64 MWe, power plant is under construction in Olkaria Northeast field.

Many studies have been carried out on the fluid chemistry of the Greater Olkaria geothermal system Arnórsson et al., 1990; Karingithi (1992, 1993, 1996, 1999, 2000); Kenya Power Company (KPC) (1982a, 1982b, 1984, 1988, 1990); Muna (1982, 1990); and Wambugu (1995, 1996). Hydrothermal alteration in the Olkaria geothermal system, has been studied by Browne (1978, 1984), Leach and Muchemi (1987), Muchemi (1992, 1993), and Omenda (1992, 1994, 1998).

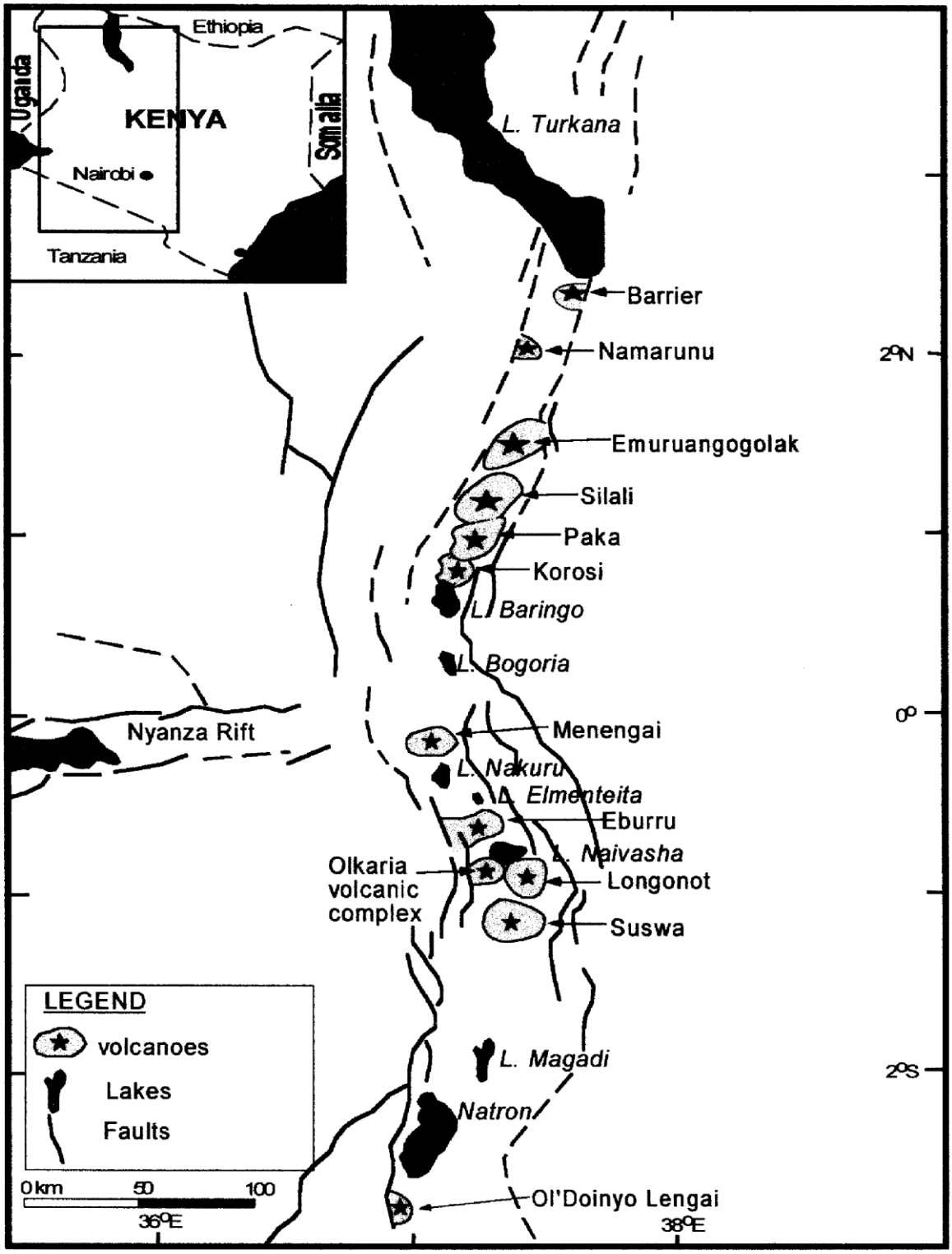

Figure 1.1: Map of the Kenya rift faults showing the major Quaternary central volcanoes and location of the Olkaria volcanic complex (KenGen, 1999)

2.0 HISTORY OF GEOTHERMAL DEVELOPMENT

Exploration for the geothermal resource in the Olkaria region started in the 1950s when two wells, X-1 and X-2, were drilled in 1956 (KPC 1984). The wells were sited on the basis of the extensive surface manifestation near the well sites. Low pressure steam was encountered at relatively shallow depth, and drilling of well X-1 was terminated at 502 m where the highest temperature measured was 120°C. Well X-2 was drilled to 1034 m with a maximum measured temperature of 235°C. However, the well proved difficult to discharge and produced low enthalpy fluid at low wellhead pressure. After the discharge test, the maximum temperature was 245°C at 940 m. Systematic exploration in the area began in 1970 through bilateral and multilateral agreements of UNDP (United Nations Development Programme) and Government of Kenya. Drilling re-commenced at well OW-1 in 1973. Although the well intersected low temperatures, subsequent drilling 3 km northeast of the well site (OW-2) confirmed the existence of a high-temperature hydrothermal system, and further drilling was confined to this area, which is the current Olkaria East production field (Figure 2.1).

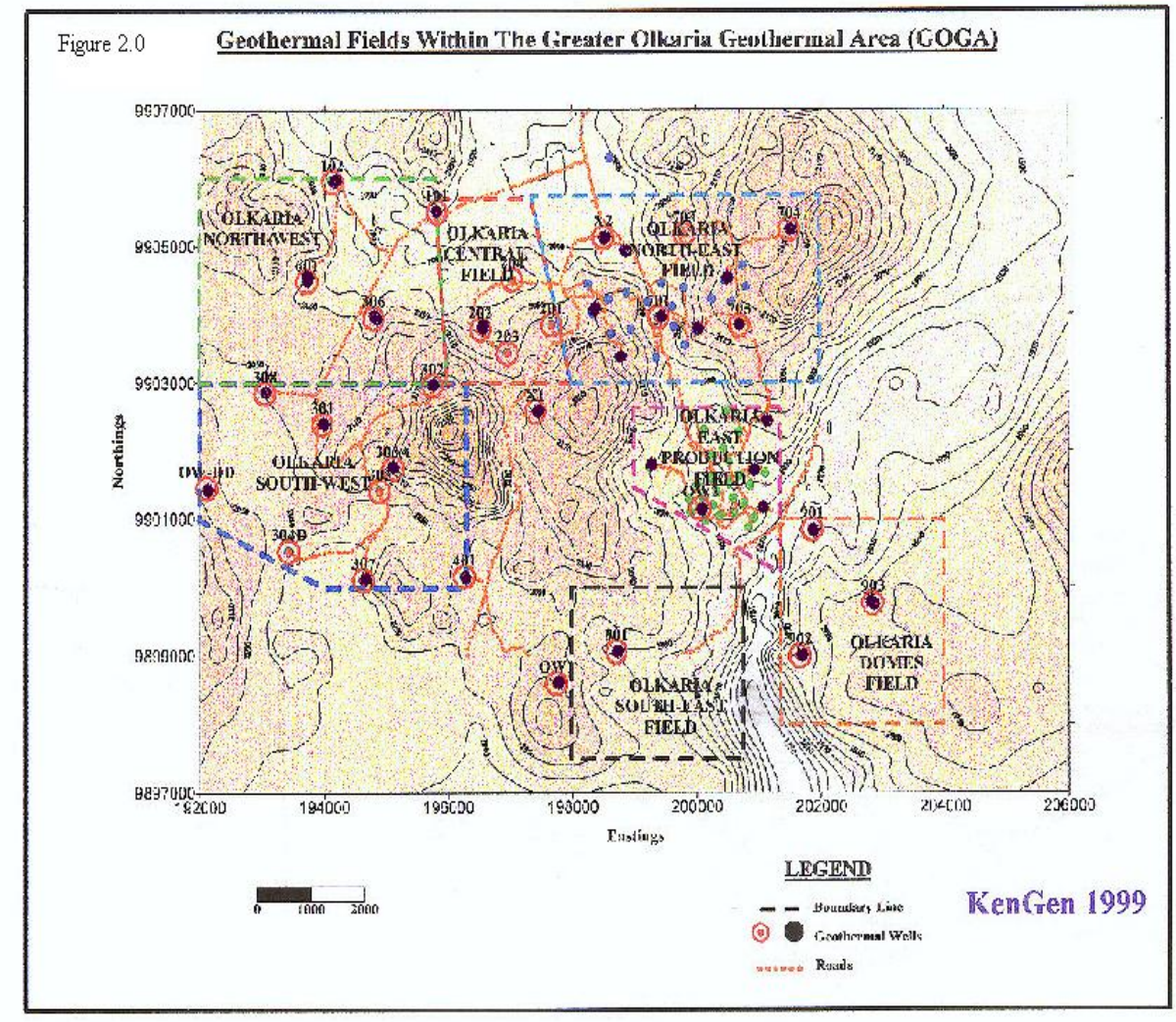

Figure 2.1: Geothermal fields within the Greater Olkaria geothermal area (KenGen 1999)

A more ambitious exploration programme started in the early 1980s when additional resistivity surveys and re-interpretation of older data indicated the possible existence of a major upflow zone of hot fluid to the northwest of the Olkaria East production field. Coupled with geological and geochemical data, four deep exploration wells were sited, OW-101, OW-201, OW-301, and OW-401 (KPC 1984). In 1985, four more wells were drilled, OW-302, OW-501, OW-601, and OW-701 (Ojiambo, 1990). From the data accrued from the eight wells above, a field development and reservoir exploitation strategy was formulated. A decision to continue exploration in both the Olkaria Northeast and Olkaria West was made. Four more exploration wells were drilled in Olkaria Northeast in 1987 and 1988, namely; OW-702D, OW-703, OW-704, OW-705 and OW-706. Four more wells; OW-303, OW-304D, OW-305 and OW-306, were drilled in Olkaria West in 1989. Production drilling for a 64 MWe power plant in the Northeast commenced in 1988 and was completed in 1991. The power plant is currently under construction, and expected commissioning date is Jan 2003. Two more exploration wells were drilled in Olkaria West, OW-307 and OW-308. The field is currently owned and operated by one of the Independent Power Producers, Orpower 4 Inc., with a combined cycle power plant of 13 MWe. Expansion of the power plant to 64 MWe or more is underway.

During the exploration, appraisal, and production stages of the above fields, a total of 102 wells have been drilled to depths ranging from 503 m in well X-1 to 2800m in well OW-601. Therefore, a large database of well information is available to assist in the understanding of the reservoir. Interpretation of geochemical, reservoir, geological, and geophysical data show that there are three main upflow zones located in the Olkaria West Field, Olkaria Northeast field and in the Olkaria Domes field (KenGen, 1999; Ofwona, 2002).

3.0 GEOLOGICAL FEATURES AND PHYSICAL RESERVOIR CHARACTERISTICS

3.1 Geology and stratigraphy

Regional Geology

The Kenya Rift Valley system is part of the 3,000 km long, East African Rift Valley system, which extends from southern Mozambique through Tanzania, Kenya and Ethiopia to join the Red Sea and the Gulf of Aden rifts at the Afar triple junction (KenGen 1998). The evolution of the Central Kenya Rift stress field and the resultant faults has been discussed by Strecker et. al., (1990). The Olkaria volcanic complex, Figures 2.1 & 3.1, is one of several major volcanic centres in the Central Kenya Rift of the East African Rift System, associated with an

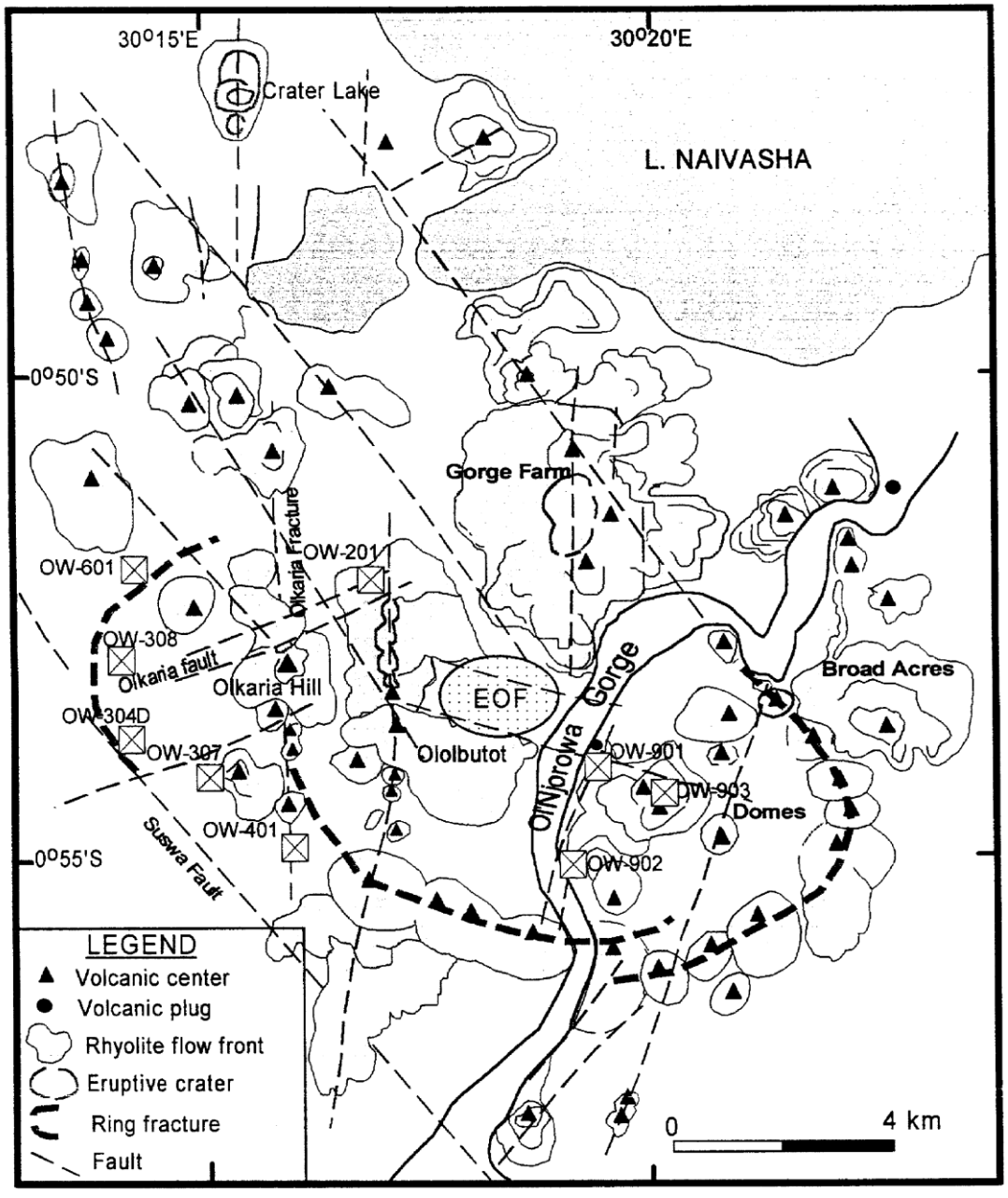

FIGURE 3.1: Volcano-tectonic map of the Greater Olkaria geothermal area (KenGen 1999)

area of Quaternary silicic volcanism. Twelve similar Quaternary volcanic centres occur in the axial region of the rift and are potential geothermal resources. These include, Suswa to the south, Longonot to the east, Eburru, Menengai, Korosi, Paka, Silali, Emuruangogolak, Namarunu and Barrier all to the North of Olkaria geothermal system (Muchemi, 1999; Omenda, 1998; Omenda et al., 1993; Riaroh and Okoth, 1994).

Surface Geology

The surface geology of Olkaria volcanic complex consists of mildly peralkaline (comenditic) rhyolite domes, lava flows, air fall pumices, and minor lake sediments, peripheral basalts and hawaiites (Macdonald et al., 1987). In the Olkaria area, the surface to about 1400 m a.s.l. is covered by quaternary comendites, pantellerites and an extensive cover of pyroclastic fall from the nearby Longonot and Suswa volcanoes. Volcanic eruption centres are structurally controlled, Figure 3.1. The main centres are the Olkaria hill, Ololbutot fault zone and the Gorge Farm area. The most recent volcanism is associated with the Ololbutot rhyolite flow, which is about 250 ± 100 years BP (Omenda, 1998; Clarke et al., 1990).

Subsurface Geology

The subsurface geology of the Olkaria geothermal field can be divided into five broad lithostratigraphic groups based on age, tectono-stratigraphy, and lithology. The formations are: The Mau Tuffs, Plateau Trachytes, Olkaria Basalts, Upper Olkaria Volcanics and minor intrusives, as shown in Figure 3.2 (Muchemi, 1999; Omenda, 1998). A structural N-S running boundary passes through the Olkaria Hill that divides the Greater Olkaria area into east and west stratigraphic zones. The geothermal reservoir to the east of the Ol Olbutot Fracture Zone is hosted within the Pleistocene Plateau Trachytes while in the west it is within the Pliocene Mau Tuffs, Figure 3.2.

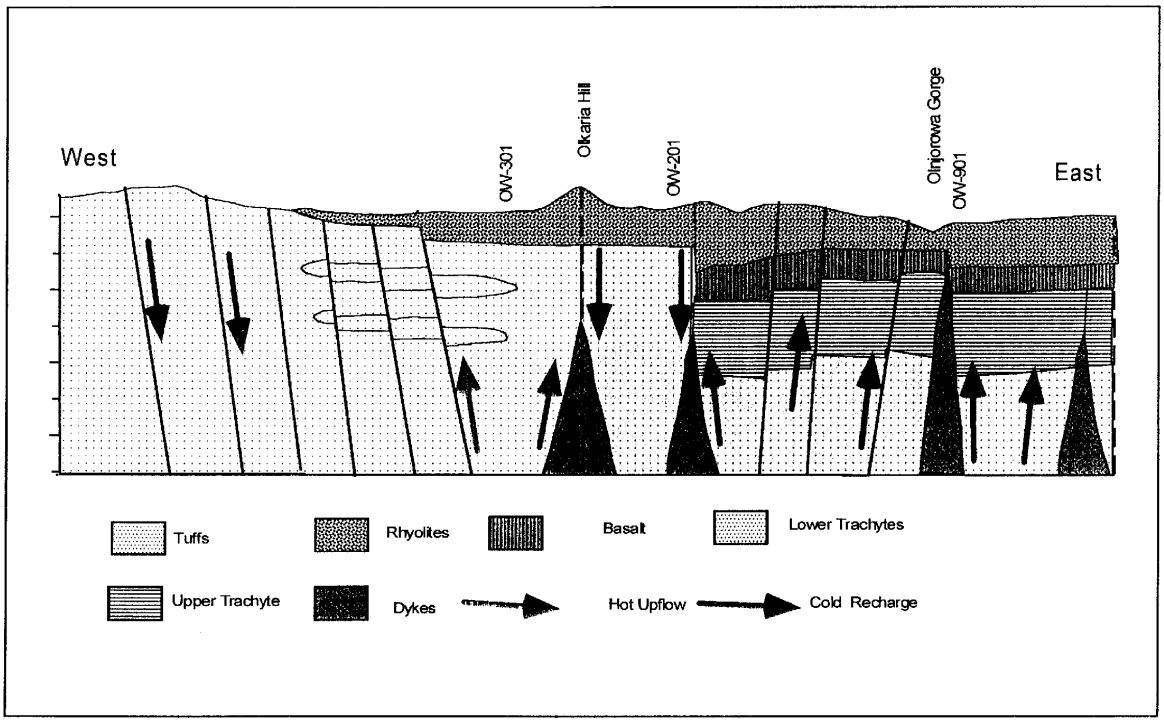

FIGURE 3.2: E-W geological cross section (Muchemi, 1999; Omenda, 1998)

Structures

The regional structures in the area are represented by; the Gorge Farm fault, the Suswa lineament and the ENE trending Olkaria fault zone. The main recharge paths to the Greater Olkaria geothermal area are NNW-SSE, ENE-WSW faults and NW-SE east dipping major rift faults exposed on the Mau escarpment. Reactivated N-S rift floor faults and fractures control axial groundwater flow through the geothermal system, but they have a shallower influence than the major rift forming faults that provide deep recharge (KenGen, 1998; Muchemi, 1999; Omenda, 1998, Clarke et al., 1990). Seismic data indicate that there is active movement along some of these faults (Simiyu et al., 1997). Mungania (1992) has demonstrated that most of the recent lava flows are associated with the N-S striking faults and the ring structure. These faults are thought to have numerous dyke swarms below the surface. Some of the dykes are well exposed in the Ol Njorowa gorge. Influence of the reactivated N-S rift floor faults and fractures on reservoir characteristics is shown by the temperature inversions that are common in most wells drilled close to the exposed N-S faults, e.g., wells OW-1, OW-201, and OW-401 (Omenda, 1998).

3.2 Hydrothermal minerals

Muchemi (1999) and Omenda (1998) have summarized studies of hydrothermal alteration of rocks penetrated by wells drilled into the Olkaria geothermal system. Hydrothermal minerals present include kaolinite, biotite, hydrobiotite, vermiculite, chlorite, chlorite-illite, illite-smectite, smectite, epidote, calcite, quartz, fluorite, anhydrite, Fe-oxides, prehnite, wairakite, stilbite, pyrite, adularia, albite, sphene, leucoxene, actinolite, garnet and talc. The most common secondary minerals are the clay minerals, fluorite, anhydrite**,** calcite, pyrite and iron oxides. Clay mineral analysis shows that the prevailing clays in the east above 1000 m a.s.l. are smectite and chlorite, whereas in the west, illite is the more dominant (Leach and Muchemi, 1987). At depths below 1000 m a.s.l., the dominant clay is interlayered chlorite-biotite and biotite. In general, the clay grading with depth in the east is smectite-chlorite-biotite and in the west smectite-illite-chlorite-biotite. Epidote has been observed to be closely associated with basalts and is more abundant in the eastern fields than in the western fields.

3.3 Pressure, temperature and permeability

The temperature and pressure distribution across the entire field has been studied and indicates that fluid movement in the Olkaria geothermal system is associated with tectonic structures. The highest temperature recorded is 340°C at 2000 metres depth in well OW-901 in Olkaria Domes. The Olkaria East reservoir is two-phase, at least to the depth penetrated by the deepest wells. High temperatures are also observed in Olkaria West, Olkaria Northeast and Olkaria Domes while lower temperatures are observed in Olkaria Central, Figure 3.3 (Ofwona, 2002). The pressures decrease both eastwards and westwards from respective peaks towards Olkaria Central. Within the Olkaria Central and Northeast the pressures decline southwards towards well OW-401 and towards Olkaria East, respectively (Ouma, 1999). The ENE-WSW trending Olkaria fault zone is the most important permeable structure in the whole of Olkaria geothermal area. A permeability thickness (Kh) product of more than 10 Darcy-meters is common in the vicinity of this fault. The fault transects the Northeast and West fields, where it forms the most productive part of the system (Figure 3.1). This fault zone forms a hydrologic divide. The geothermal reservoir in the north (including Olkaria Domes) is liquid dominated and has no steam cap, whereas south of the fault the reservoir is a liquid–dominated two phase system overlain by a steam dominated zone (Ambusso and Ouma, 1991; KenGen 1999).

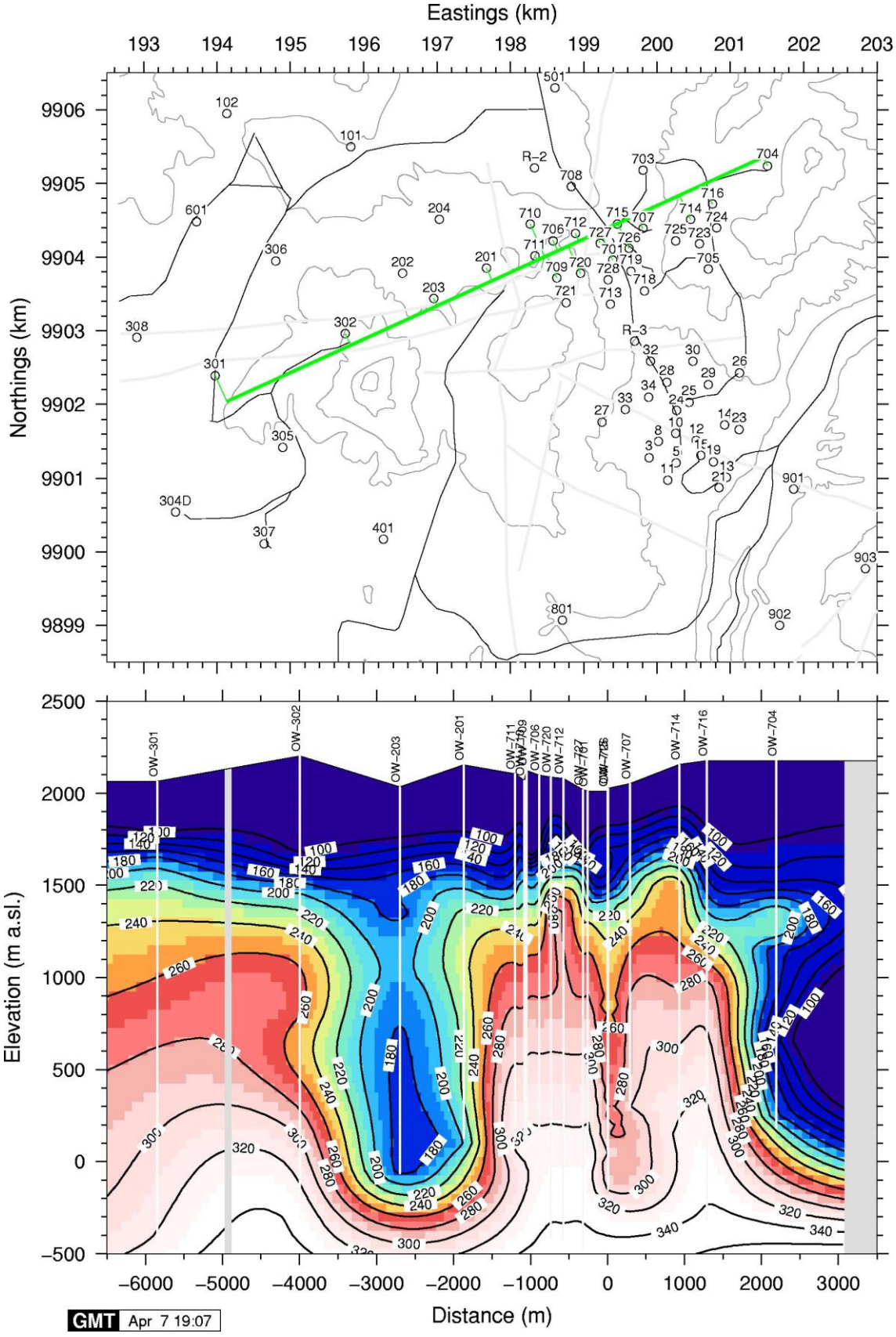

FIGURE 3.3: E-W temperature cross section (Ofwona 2002)

3.4 Well discharge enthalpy.

The Olkaria geothermal wells have discharge enthalpy ranging from less than 1000 kJ/kg to saturated steam enthalpy of 2750 kJ/kg (Table 1). Most of the wells in the Olkaria East production field have excess discharge enthalpy, i.e., the enthalpy of the discharged fluid is higher than that of steam-saturated water at the respective aquifer temperature. Excess enthalpy may be the consequence of several processes. It may be a reflection of the high enthalpy of two-phase aquifer fluid. Alternatively, it can be caused by flow of heat to the fluid flowing into wells from the rock in the depressurisation zone around these wells or by partial phase segregation of the water and steam in this zone according to Arnórsson et al. (1990).

3.5 Fluid composition

For this study, twenty-six (26) wells from five of the seven fields within the Greater Olkaria area were selected for water and steam sampling. Samples considered are those in Karingithi (2000) and samples collected specifically for this study in 2001. The data is shown in Table 1. The fluid chemistry of each individual field has been studied and characterised. Application of the $Cl\text{-}SO_4\text{-}HCO_3$ ternary diagram shows that the wells in the Olkaria West field discharge sodium-bicarbonate type water, while the wells in Olkaria East and Olkaria Northeast fields discharge alkaline sodium chloride type water. Olkaria Central and Olkaria Domes wells discharge a mixture of the sodium chloride and sodium bicarbonate end member fluid types (Karingithi, 2000).

The total concentration of dissolved solids (TDS) in the fluid discharged by wells in the Greater Olkaria geothermal system is low, compared to most high-temperature geothermal systems in the world. The chloride concentration in the water at the weirbox varies between 100 and 1100 ppm, being lowest in well OW-304D and highest in well OW-10. The wells in Olkaria East and Olkaria Northeast tend to be highest in chloride. This could be the consequence of up-flow of deep high-temperature geothermal fluid, although progressive boiling by heat flow from the rock may also contribute in the Olkaria East field well discharges (Karingithi, 2000). In the Olkaria West field the chloride concentrations are quite low (100-200 ppm) except in well OW-305, which discharges water similar to that discharged from the wells in the Olkaria East and Northeast fields (530-750 ppm Cl at the weirbox, Wambugu, 1996). Well OW-305 is thought to be tapping the up-flow fluid for Olkaria West field, while other wells in the same field are thought to discharge fluid which has been diluted by either steam condensate or shallow ground water.

The water at the weirbox is alkaline (pH 8.1 to 9.9 as measured at 20°C) and is relatively high in bicarbonate, ranging from 90 ppm in Olkaria East to 13,000 ppm in some of the wells in Olkaria West (Table 1). The high bicarbonate in Olkaria West is considered to be a consequence of CO_2 supply to the geothermal fluid and a subsequent reaction between the carbonic acid and the minerals of the rock, which act like bases, thus converting some of the carbon dioxide to bicarbonate. The source of CO_2, at least in Olkaria West, is considered to be predominantly from the magma heat source of the geothermal system although carbon present in the rock may also contribute.

The CO_2 concentration in the steam phase varies from 0.67 mmoles/mole of steam in well OW-30 in the Olkaria East field to 206.5 mmoles/mole of steam in well OW-304D located in Olkaria West field. The concentration of H_2S varies from 0.009 mmoles/mole of steam in well OW-902 in Olkaria Domes, to 0.168 mmoles/mole of steam in well OW-20 in the

Olkaria East field. The H_2 concentration varies from 0.000 in well OW-202 in Olkaria Central field to 0.095 mmoles/mole of steam in well OW-23 in Olkaria East. The ascending order for both H_2 and H_2S is Olkaria Domes less than Olkaria Central, which is less than Olkaria West, followed by Olkaria Northeast and finally Olkaria East, Table 1. The variation of methane gas concentration follows the same trend as CO_2, it varies from 0.000 in well OW-30 to 0.031 mmoles/mole of steam in well OW-304D in Olkaria West. The N_2 gas concentration, which is an indicator of inflow of shallow atmospherically contaminated water into the well, has a minimum value of 0.016 mmoles/mole of steam in well OW-202 located in Olkaria Central and a maximum value of 0.342 mmoles/mole of steam in well OW-903 located in Olkaria Domes.

Isotope analysis of samples taken within the geothermal system indicates that, although they are close to the Kenya Rift Valley meteoric line (Kenya rain line – Clarke et al., 1990), the fluid source for individual fields is different (Karingithi 2000). Water samples taken to the east of the Ol Olbutot fault are enriched in both ^{2}H and ^{18}O relative to local precipitation. Since the samples plot close to or on the local meteoric line, this implies that the water evaporated before infiltrating into the bedrock of the geothermal system. The more negative deuterium values of the aquifer water in Olkaria West and Central ($\delta^{18}O$ from –0.75 ‰ to –5.4 ‰ and $\delta\ ^{2}H$ from 0.38 ‰ to –14.92 ‰) indicated a different recharge area for the Olkaria West sector compared to the Olkaria East sector.

4.0 SAMPLING AND ANALYSIS

4.1 Water samples

For this study, twenty-six (26) wells from five of the seven fields were selected for water and steam sampling. A chromium steel Webre separator was used to collect the steam samples from the well-head two-phase flow pipe of appraisal and exploration wells that do not have the standard steam cyclone separators. The Webre separator was connected to the sampling valve provided on the two-phase flow pipe. The water samples were then collected from the weirbox after separation of the two-phase fluid through the atmospheric silencer. For the production wells in the Olkaria East field, a stainless steel tubing was connected to the steam pipe at the sampling valve provided immediately after the cyclone separator. Steam samples were collected into two gas-sampling bulbs, which had been evacuated and weighed before and after introducing 50 ml of freshly prepared 4 M NaOH solution in the laboratory. After sampling, the gas bulbs were weighed and hence the weight of the steam condensate collected was accurately determined. Steam samples were used for the determination of CO_2, H_2S, H_2, CH_4, N_2, and O_2 (detected in atmospherically contaminated samples) in the separated steam. A Varian Gas Chromatograph was used for the analysis of the non-condensable gases (H_2, CH_4, N_2, and O_2), while CO_2 and H_2S were analysed by titration (Arnórsson et al., 2000).

Water samples were then collected from the weirbox at atmospheric pressure, filtered on site through a 0.2 µm millipore membrane (cellulose acetate) into low density polyethylene bottles using a polypropylene filter holder. The entire filtration apparatus was thoroughly rinsed with deionised water and sample fluid before collecting a sample. Two 100 ml portions of the sample were collected for both major cations and trace metal analysis. In each of the bottles, 1 ml of suprapure concentrated nitric acid was added. A 100 ml sample was collected for the sulphate analysis, and to this sample, 1 ml of 1% zinc acetate solution was added to remove H_2S. Hydrogen sulphide was analysed on site by titration with 0.001 M mercuric acetate solution using dithizone as indicator (Arnórsson et al., 2000). Two amber glass bottles, 100 ml and 250 ml, with special caps that prevent entrapment of an air – bubble under the cap were used to collect samples for the determination of deuterium and oxygen-18, pH and total carbonate carbon. Samples for the analysis of Cl and F were not treated.

Total carbonate carbon and pH were determined in the laboratory immediately after sample collection from the field (1-2 hours) with a Metrohm titrator and a Metrohm rapid response pH electrode (Arnórsson et al., 2000). To prevent any CO_2 loss from the bottle, which can cause changes in pH during measurement, the pH electrode was placed directly into the amber bottles, which had a top with a hole of almost equal diameter as the electrode. The major aqueous cations (Na, K, Ca, Mg, Al, Fe) plus Si, SO_4, B were analysed on a Thermo Jarrel Ash ICP-AES and Ion Chromatography was used to analyse Cl and F. Analyses of oxygen-18 and deuterium were carried out on a Finnegan MAT 251 mass spectrometer (Epstein and Mayeda, 1953).

4.2 Electron microprobe analysis

Thin sections were prepared from rock cuttings recovered from eight geothermal wells at Olkaria at various depths, as tabulated in Table 2 below. Twenty-six thin sections of rock cutting chips were prepared and smoothened for the microprobe analysis. The microprobe is a recently updated ARL-SEMO (Scanning Electron Microprobe Quantometer). It has four fixed channels (Si, Al, Fe, Ca) and three scanners. The analysis was done at 15 kV with a

sample current of about 15 nA and a beam diameter of 2-3 micrometers. The software is from John Donovan at Berkeley and uses ZAF correction. The standards used were natural minerals and glasses of similar composition as the samples analysed. A total of 1532 determinations were carried out to determine major element mineral composition. A summary of the results showing the chemical compositions of epidote and garnet minerals as deduced from the micro-probe analysis is given in Table 3. The methodology of obtaining the chemical formulae is as outlined in Deer et al., (1992) and Droop, (1987).

Table 3 shows the tabulated analysis results of the chemical composition of the garnet and the epidote solid solutions. The andradite/grossular solid solution varies between an activity of grossular of 0.36 to 0.51. The average activity of grossular and clinozoisite of 0.43 and 0.07 respectively were used in this study.

5.0 CALCULATION OF AQUIFER FLUID COMPOSITION, AQUEOUS SPECIATION AND MINERAL SOLUBILITY

5.1 Aquifer fluid composition

Aquifer fluid compositions were calculated with the aid of the WATCH speciation programme (Arnórsson et al., 1982), Version 2.1A, (Bjarnason, 1994). Most of the wells in Olkaria geothermal field have excess enthalpy, i.e., the enthalpy of the discharged fluid is higher than that of steam saturated water at the respective aquifer temperature. This causes uncertainty as how to obtain aquifer water composition from analysis of water and steam samples collected at the wellhead. Excess enthalpy may be a consequence of several processes (Arnórsson et. al., 1990). One involves partial segregation of the water and steam phases in the depressurization zone around the wells so that the water fraction is partially retained in the aquifer, while the steam flows into the wells. The second process involves flow of heat from the aquifer rock in the depressurization zone to the fluid flowing into the wells. The pressure drop causes boiling of the liquid phase, which results in cooling, and hence a positive temperature gradient is created between the aquifer rock and the flowing fluid. Thirdly, excess enthalpy could also be a reflection of high steam fraction of the initial aquifer fluid. Difficulties in evaluating the relative contribution of these boiling processes to the excess enthalpy of well discharges lead to uncertainties as how to calculate the chemical composition of the aquifer fluid from analytical data on water and steam samples collected at the wellhead.

The enthalpy of saturated steam varies with temperature. It reaches maximum around 235°C and in the range 180-270°C (10-55 bars abs. vapor pressure) it has a value close to this maximum but at lower and higher temperatures it drops significantly. As a consequence of this, the steam to water ratio (enthalpy) of a fluid has little effect upon vaporization of the water during depressurization in the pressure interval 10-55 bars abs. but at lower and higher pressure, vaporization by depressurization increases with increasing steam fraction of the fluid. Most of the Olkaria wells have aquifer temperatures of less than 270°C so enhanced water evaporation above 270°C due to excess enthalpy can be ignored. On the other hand, the excess enthalpy may significantly enhance evaporation of water flowing into the weirbox, particularly for exploration and appraisal wells that do not have a steam wellhead separator.

The procedure used to calculate aquifer fluid compositions for the exploration and appraisal wells was as follows: (1) Gas concentrations in steam were reduced corresponding to boiling from the sampling pressure to atmospheric pressure, (2) the composition of water and steam were calculated at 10 bars abs vapour pressure using the measured discharge enthalpy value with the aid of the WATCH chemical speciation program (Arnórsson et al., 1982), version 2.1A, (Bjarnason, 1994) and (3) the aquifer component concentrations were calculated at a selected aquifer temperature assuming no effect of the excess enthalpy on the vaporization of the water phase.

Pressure logging indicates that the reservoir in the Greater Olkaria geothermal area is liquid dominated in terms of volume except for the steam zone that caps the liquid reservoir in the Olkaria East Production Field. This leaves phase segregation in the aquifer as the most important process in generating excess enthalpy well discharges although heat transfer and initial high aquifer steam fraction may also contribute. Aquifer component concentrations have been calculated on the assumption that this process accounts solely for the excess enthalpy.

5.2 Aqueous speciation

Having selected a satisfactory model to calculate component concentrations in the producing aquifers beyond the depressurization zone around wells, the WATCH chemical speciation program was used to calculate individual aqueous species activities and mineral saturation in the initial aquifer fluid. The data base for these calculations is that presented by Arnórsson et al. (1982) except for gas solubility, Al-hydroxide, ferrous and ferric hydroxide dissociation constants, which were taken from Arnórsson et al. (1996), Arnórsson and Andrésdóttir (1999), and Diakonov and Tagirov (2002), respectively.

5.3 Thermodynamics of minerals, aqueous species and mineral solubility constants

The saturation state of the aquifer water at Olkaria has been assessed for various end-member hydrothermal minerals and mineral buffers found in the reservoir rock. The minerals considered include andradite, calcite, clinozoisite, epidote, grossular, magnetite, pyrite, pyrrhotite and wollastonite. The thermodynamic properties (ΔG_f^o, S^o, V^o, C_p^o) of these minerals were selected from the data set of Robie and Hemingway (1995) except those for clinozoisite and epidote Table 4. The standard enthalpy of formation from the elements ΔH_f^o for these two last listed minerals was taken from Smelik et al. (2001), but S^o, V^o, C_p^o from Holland and Powell (1998a & b). The ΔG_f^o for these minerals was obtained from the selected enthalpy and entropy values and the absolute entropies for the elements from CODATA. The ΔG_f^o values at 25°C and 1 bar so obtained are –6,487,370 J mol^{-1} and –6,075,110 J mol^{-1}, for clinozoisite and epidote, respectively.

The solubility constants for individual minerals, mineral pairs and mineral buffers considered have been expressed in terms of the reactions given in Tables 5 to 7. The thermodynamic properties of the aqueous species appearing in these reactions were extracted from two sources. Ca^{+2}, Fe^{+2}, OH^-, CO_{2aq}, H_2S_{aq}, H_{2aq}, and H_2O_l were calculated with the aid of the SUPCRT92 computer program (Johnson et al., 1992) using the slop98.dat data set. The thermodynamic properties for $Fe(OH)_4^-$ and H_4SiO_4, were taken from Diakonov et al. (1999) and Gunnarsson and Arnórsson (2000).

The activity product (Q) for a mineral or a mineral buffer can be expressed by

$$Q = \prod_i a_i^{\nu_i} \qquad (1)$$

where $\prod_i a_i^{\nu_i}$ is the product of all activities, a_i, each raised to the power of its stoichiometric coefficient, ν_i, which is negative for reactants and positive for products. Further, the activity of water was assumed to be unity and the activity of end-members of solid solutions proportional to their mole fraction raised to the power of the number of exchangeable sites, i.e. $a_i = X_i^n$, where X stands for the mole fraction, a for activity and n for the number of exchangeable sites in the crystal lattice.

The temperature dependence of the equilibrium constants for individual mineral-solution reactions and mineral buffers considered for the present study is consistent with the selected thermodynamic data. They are consistent with end-member mineral compositions, i.e. the activity of the minerals is taken to be unity and they are valid in the range 0-350°C at water saturation pressure (P_{sat}). This is an acceptable approximation for Olkaria as wells follow the boiling point with depth curve.

5.4 Errors in calculated mineral solubility constants

Error limits have been evaluated for log K, log Q, and individual activities per mole of gas, cation or anion. For log K, the errors are accrued from the experimentally derived thermodynamic data available for individual mineral phases, liquid water and aqueous gases included in the respective mineral buffer equilibrium reactions. The errors for standard Gibbs energy of formation of individual minerals were retrieved from Robie and Hemingway, (1995), and Smelik et al., (2001). The cumulative error for all the reactions in Table 5 and 7 was less than 2 log K units except for two reactions involving gro-pyr-mag-epi-H_2S and gro-mag-epi-wol-H_2. The cumulative error for these two reactions was between –2.45 to –9.75 log K units, in the temperature range of 150°C to 350°C, which is the temperature range measured in the aquifer of most Olkaria wells whose discharge samples are considered. The stoichiometry in the two reactions account for the large error observed.

Analytical errors are minor when compared to errors resulting from thermodynamic data. The waters considered in this study are quite dilute and hence the values for individual ion activity coefficients are precise. The calculated aqueous fluid composition carries some errors, which cannot be quantified. The magnitude depends on how accurately the model used to calculate the aquifer composition matches the boiling processes in the aquifer. Probably, the largest error is in the calculated aquifer pH. Additionally, precipitation processes between the aquifer and the wellhead, which cause well discharge compositions to differ from aquifer fluid composition, produce systematic errors. Errors in the calculated saturation indices depend on the same errors as those for the mineral solubility constants, analytical errors for the aqueous components plus errors involved in calculating the activities of the aqueous species used to express the various mineral dissolution reactions.

6.0 MINERAL BUFFERS CONTROLLING REACTIVE GAS CONCENTRATIONS

The principal objective of this contribution is to evaluate if equilibrium is closely approached between certain mineral buffers and the reactive gases, CO_2, H_2S and H_2. The minerals constituting the selected buffers have all been encountered as hydrothermal minerals within the Olkaria geothermal reservoir. Equilibration conditions have been studied with respect to individual minerals, mineral pairs and mineral buffers according to the reactions shown in Tables 5 to 7.

6.1 Calcite

The temperature dependence of the calcite equilibrium constant (K) is illustrated in Figure 6.1. The activity product (Q) of individual samples, as calculated by the WATCH speciation program, has been posted to evaluate their distribution. Twelve samples are at equilibrium within the limit of error in the calculated log K value, four are over-saturated and thirteen under-saturated. On average, the waters are under-saturated by 0.18 log Q units.

The degree of calcite saturation can to some extent be related to the calculated aquifer pH (Figure 6.2), which in turn depends to a considerable extent on the measured pH of the sample of water collected from the weirbox. Thus, well 709, which shows the highest degree of over-saturation, has anomalously high aquifer pH in relation to other wells with similar aquifer

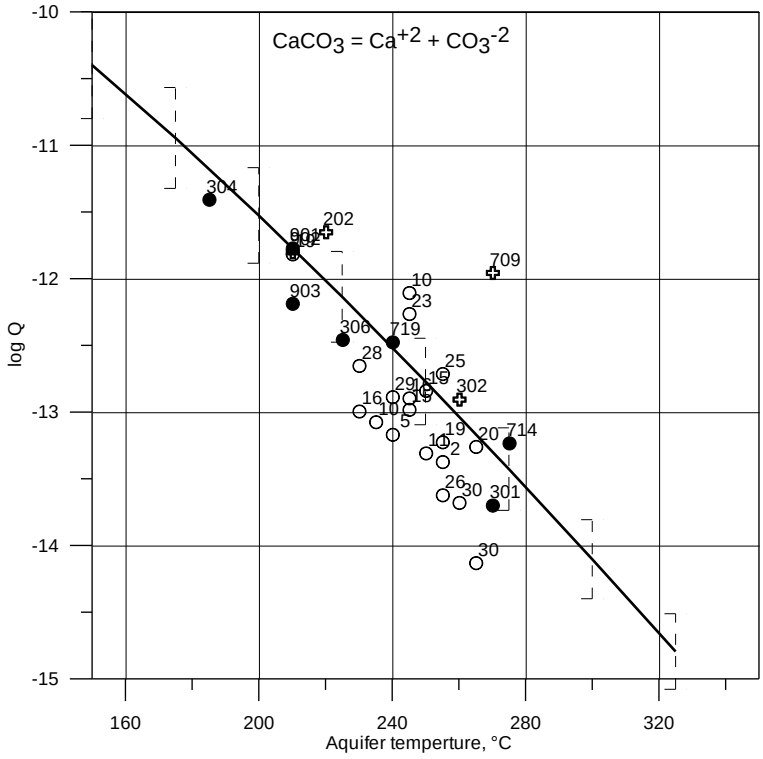

Figure 6.1: Aquifer temperature versus log Q. The continous line depicts the calcite dissolution/precipitation equilibrium constant dependence with temperature. The open circles, the black dots and the open crosses represent samples taken from Olkaria East wells, Olkaria West plus Domes, and wells considered to be marginal wells respectively. The numbers represent actual Olkaria well identification numbers.

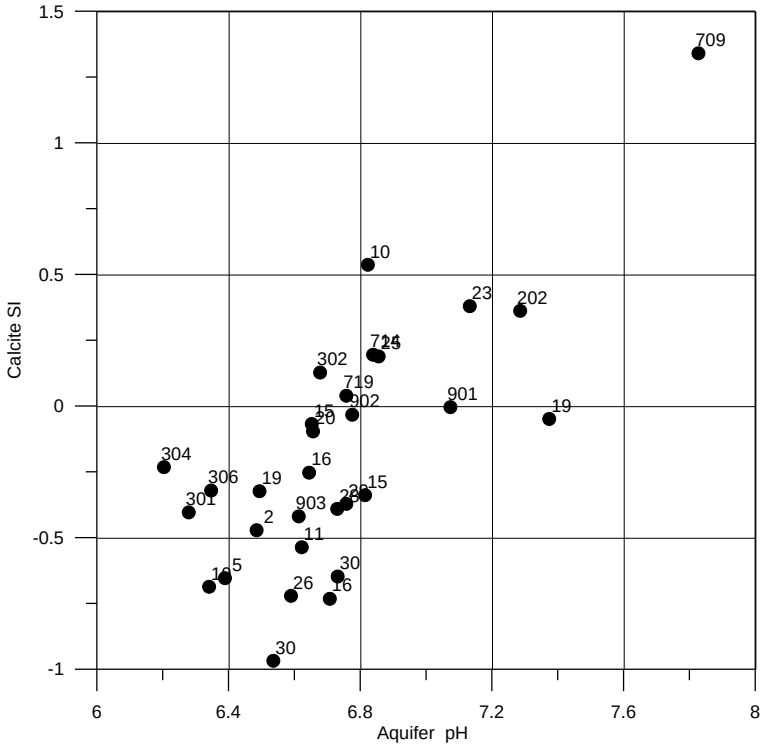

Figure 6.2: Aquifer pH versus calcite SI . Symbols and numbers, see Figure 6.1.

However, no precise methods are known to be available to estimate the initial aquifer steam fraction reliably. Evidence, however, indicates that it is minor by weight (Arnórsson et al., 1990) so it was considered to be a reasonable approximation to take it to be zero. If equilibrium steam actually exists, but its presence is ignored in calculating aquifer water composition and speciation distribution in that water, the outcome is too low aquifer water pH and too low log Q values for calcite. Calculated aquifer water pH, as a function of the quantity of equilibrium steam in the aquifer fluid (by weight) is shown in Figure 6.3 for two wells. The results indicate that the presence of only a small steam fraction (5% by weight), will yield a calculated aquifer pH that is considerably higher than the pH obtained by ignoring the existence of such steam (0.5-0.6 for the two wells for which results are shown in Figure 6.3), as was done in this study. The existence of aquifer steam will therefore lead to apparent calcite under-saturation.

High water pH can, of course, be caused by analytical imprecision but it may also be the consequence of degassing of the water in the weirbox prior to sampling or during the pH measurement. Most of the waters have a pH of 8.5 to 9.5. In this range, the pH buffer capacity of the water is limited and only a limited degassing of the water with respect to CO_2 and H_2S is needed to raise the pH substantially.

The Ca content of the geothermal water at Olkaria is low, 1-2 ppm. Upon extensive boiling of this water in the depressurization zone around wells, initially calcite saturated water becomes over-saturated leading to calcite deposition and causing the Ca content of well discharges to become lower than that of the parent aquifer water. Calcite deposition of this kind leads to low values for calculated calcite saturation index (SIcal) values, i.e. apparent calcite under-saturation, if the aquifer water was at saturation at the point where extensive depressurization boiling set in.

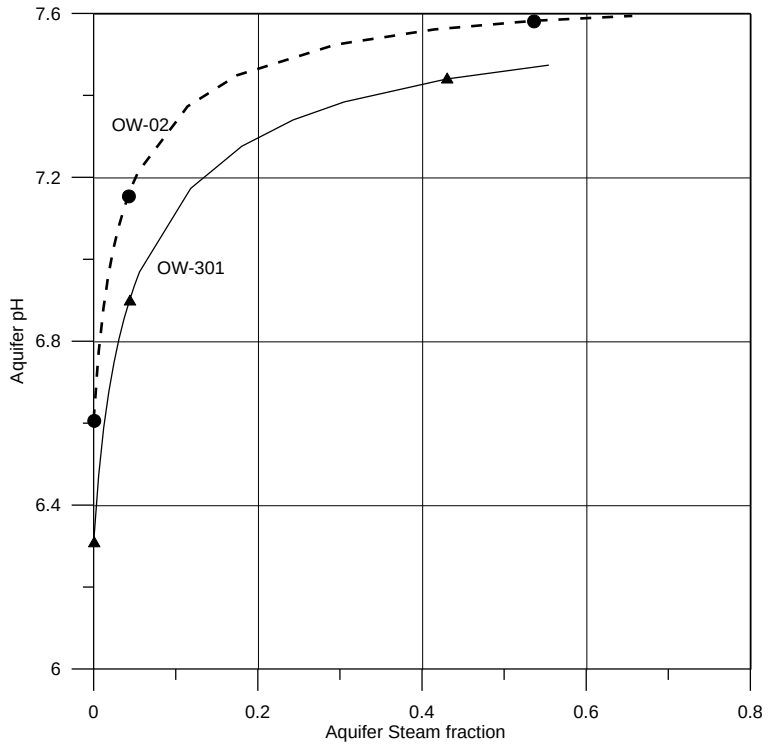

Figure 6.3: Aquifer steam fraction versus aquifer pH for well OW-2 (Olkaria East) and OW-301 (Olkaria West). Symbols and numbers, see Figure 6.1.

It is not possible to quantify the discrepancies produced in SIcal by calcite deposition in the aquifer and by ignoring the presence of equilibrium steam. At Krafla in Iceland, which has low calcium waters like Olkaria, downhole sampling has demonstrated that more than half of the Ca initially present was removed from solution to form calcite scales in the wellbore, thus causing a decrease in the log Q value by more than 0.3 units (Ármannsson, 1996). Deposition of this magnitude at Olkaria, which does not seem unlikely, together with the presence of some equilibrium steam in the aquifer of the wells studied, could shift the log Q values for calcite down by this much. It is concluded that, most of the Olkaria samples in the current study, approach calcite-solution equilibrium within the limit of error.

6.2 Clinozoisite and epidote

The temperature dependence of the equilibrium constants of clinozoisite and epidote is depicted in Figures 6.4 and 6.5. The curve for clinozoisite corresponds to an activity of 0.07 for the mineral, which is the average epidote composition in the Olkaria geothermal reservoir (see Table 3). All samples except one are, within the limit of error in the calculated logK value, at equilibrium with clinozoisite of average composition in the Olkaria reservoir. On average the aquifer water is over-saturated by 0.09 log Q units. Removal of calcium from solution by calcite precipitation upon extensive boiling between undisturbed aquifer and wellhead causes the calculated log Q values to be a little low, by twice as much as for calcite, because of the stoichiometry of the reactions. Although not proven, it may be that some Al-bearing phases could precipitate from the water upon extensive boiling. Such phases have been encountered in scales in wellbores. Such precipitation would cause calculated log Q values for the aquifer water to become too low. Errors in aqueous silica activity will contribute little to errors in calculated log Q values for clinozoisite. On the other hand, error in the retrieved aquifer water pH may be significant. Waters with the lowest aquifer pH (<6.4) tend to show the highest degree of clinozoisite under-saturation. The low calculated pH,

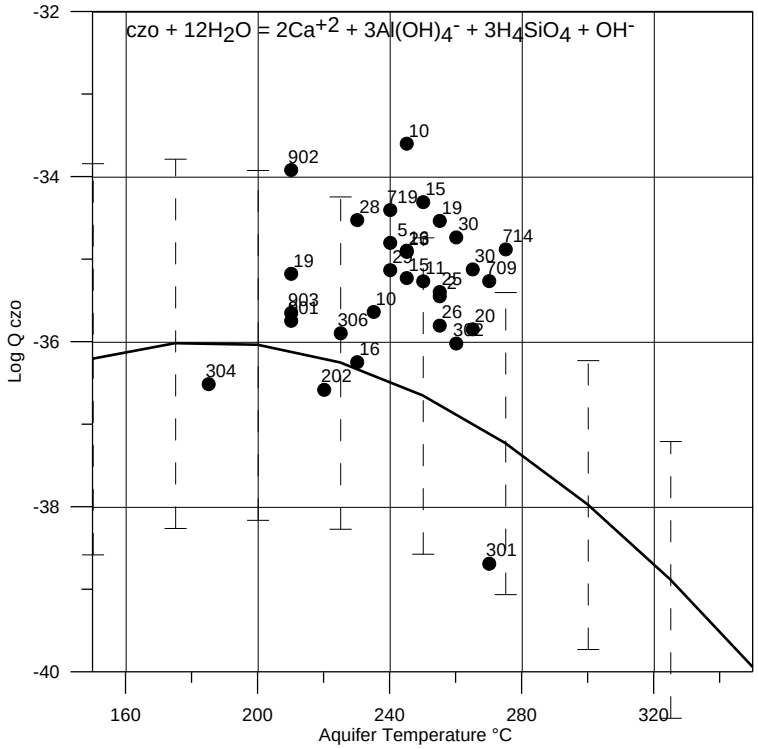

Figure 6.4: Aquifer temperature versus activity product. The continous line depicts the clinozoisite solubility equilibrium constant dependence with temperature. The activity of clinozoisite is taken as 0.07 (see Table 2 in the text). Symbols and numbers, see Figure 6.1.

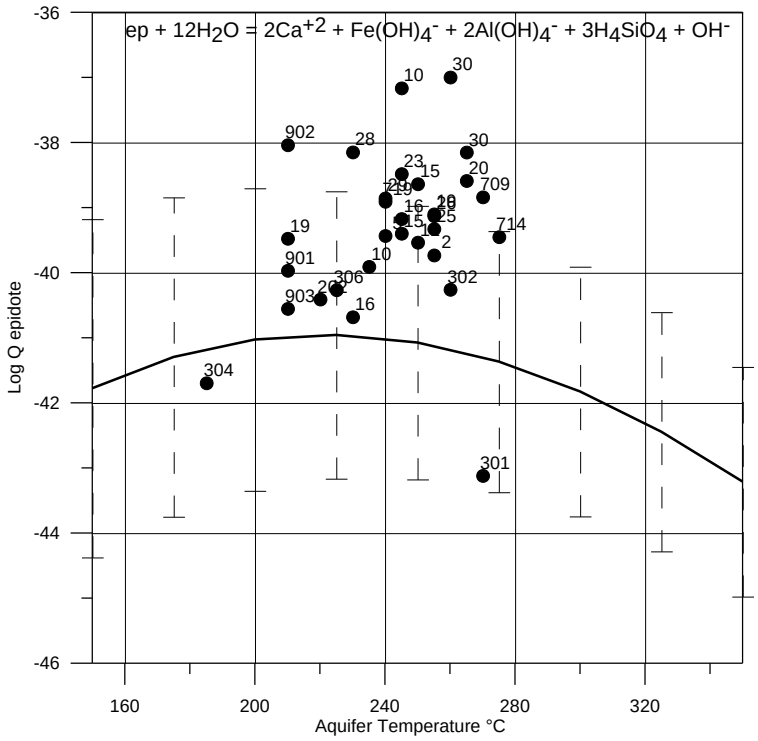

Figure 6.5: Aquifer temperature versus activity product. The continous line depicts the epidote solubility equilibrium constant dependence with temperature. Symbols and numbers, see Figure 6.1.

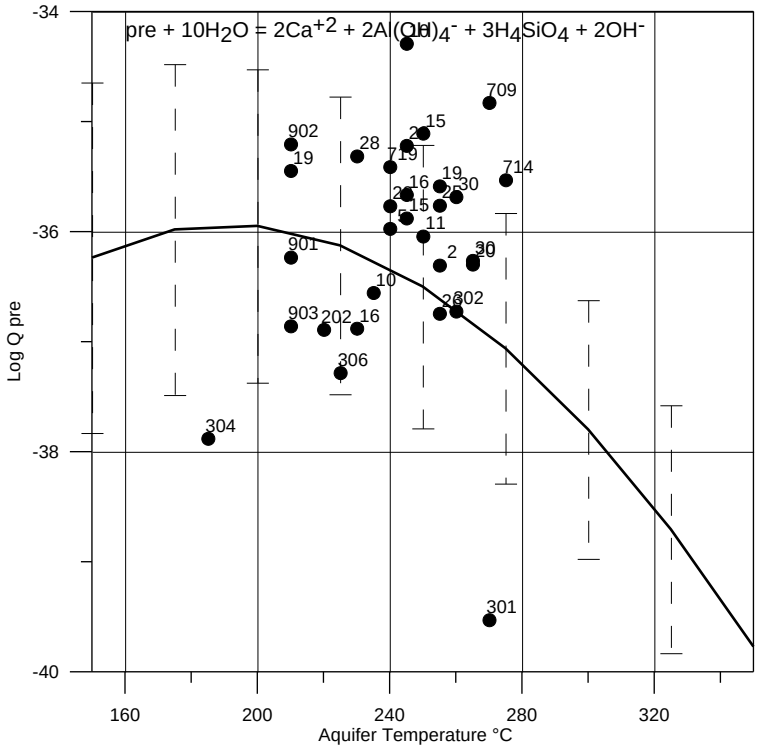

Figure 6.6: Aquifer temperature versus activity product. The continous line depicts the prehnite solubility equilibrium constant dependence with temperature. Symbols and numbers, see Figure 6.1.

which contributes to low log Q values, is probably largely the consequence of the assumption that there is no equilibrium steam in the aquifer.

The SI pattern for epidote does not differ much from that for clinozoisite. However, all the aquifer waters, except for two, have positive SIepi values, and 10 out of 30 are significantly over-saturated. On average the SIepi values are positive by 1.72 units. The calculated log Q values for epidote depend on the same parameters are those for clinozoisite and, in addition, on the calculated activity of the $Fe(OH)_4^-$ species. Thermodynamic data for ferrous and ferric hydrolysis constants are not of adequate quality. The data used here to retrieve aqueous species distributions, which are the same as those used by Arnórsson et al. (1999), lead to over-estimation of the activity of $Fe(OH)_4^-$ and a corresponding under-estimation of ferrous species activities, including Fe^{+2}. It is considered that the over-estimation of the activity of the $Fe(OH)_4^-$ species makes the log Q values systematically too high. The difference in the degree between clinozoisite (activity = 0.07) and epidote (activity = 0.93) is on average 1.63 log Q units. This numerical difference is considered to be largely due to the over-estimation of the activity of the $Fe(OH)_4^-$ species but not so much to the error in the standard Gibbs energy of formation of the two minerals. Bearing this in mind and the error in the log K value for epidote, it is concluded that the aquifer water at Olkaria is close to equilibrium with this mineral.

6.3 Prehnite

The calculated log Q values for prehnite scatter around the equilibrium curve (Figure 6.6). Twenty-four samples are at equilibrium within the limit of error in the log K value, four over-saturated and two under-saturated. On average the aquifer water are over-saturated by only

0.34 log Q units. The same parameters control log Q values for prehnite as for clinozoisite, although in different proportions. The similar average SI values for prehnite and clinozoisite suggest that the thermodynamic data on the two minerals are internally consistent within 2500-3000 J/mol, at least if the Olkaria waters have equilibrated with both minerals.

6.4 Grossular

The majority of the aquifer waters is saturated with respect to grossular of average composition (agro = 0.43) at Olkaria (Figure 6.7) within the limit of error in the calculated log K value. Five are under-saturated and three over-saturated. On average the waters are under-saturated by 1.14 log Q units. Grossular solubility is strongly pH dependent. Indeed the calculated degree of saturation is pH dependent (Figure 6.8). These results are taken to indicate that error in calculated aquifer pH contributes more to the scatter of data points in Figure 6.7 than variable departure from actual equilibrium. Low calcium concentrations in well discharges relative to those of the parent aquifer water, due to calcite deposition in the depressurization zone around wells, contribute to yield low log Q values. Taking this into account and the effect of the presence of equilibrium steam in the aquifer, which would give a higher pH, if assumed to be present, it is concluded that the aquifer water at Olkaria is close to equilibrium with the grossular of the composition occurring at Olkaria.

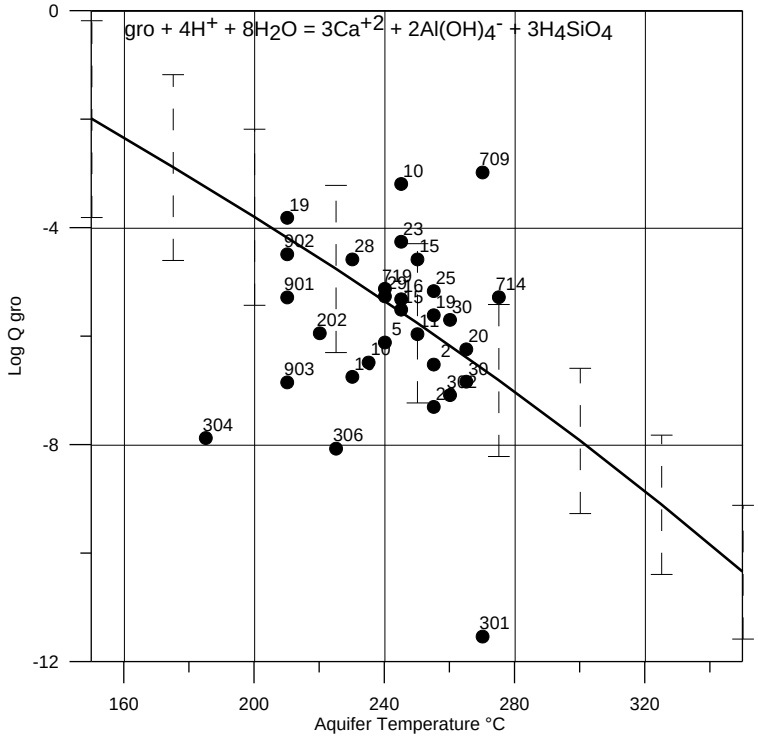

Figure 6.7: Aquifer temperature versus activity product. The continous line depicts the grossular solubility equilibrium constant dependence with temperature. The activity of grossular is taken as 0.43 (see Table 2 in the text).
Symbols and numbers, see Figure 6.1.

6.5 Magnetite, pyrite and pyrrhotite

The temperature dependence of the pyrite and pyrrhotite equilibrium constants is illustrated in Figures 6.9 and 6.10. The calculated activity products for these minerals have been posted for aquifer waters at Olkaria to evaluate their degree of saturation with respect to these minerals.

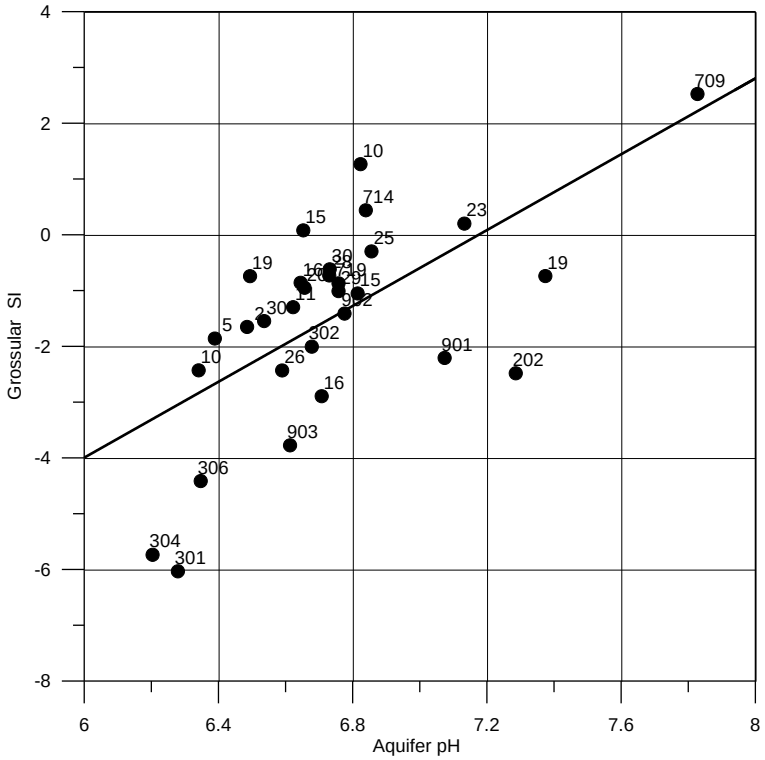

Figure 6.8: Aquifer pH versus grossular SI. The continous line depicts the best fit through the data points, with linear fit: Y = 3.3992 * X - 24.3909.
Symbols and numbers, see Figure 6.1.

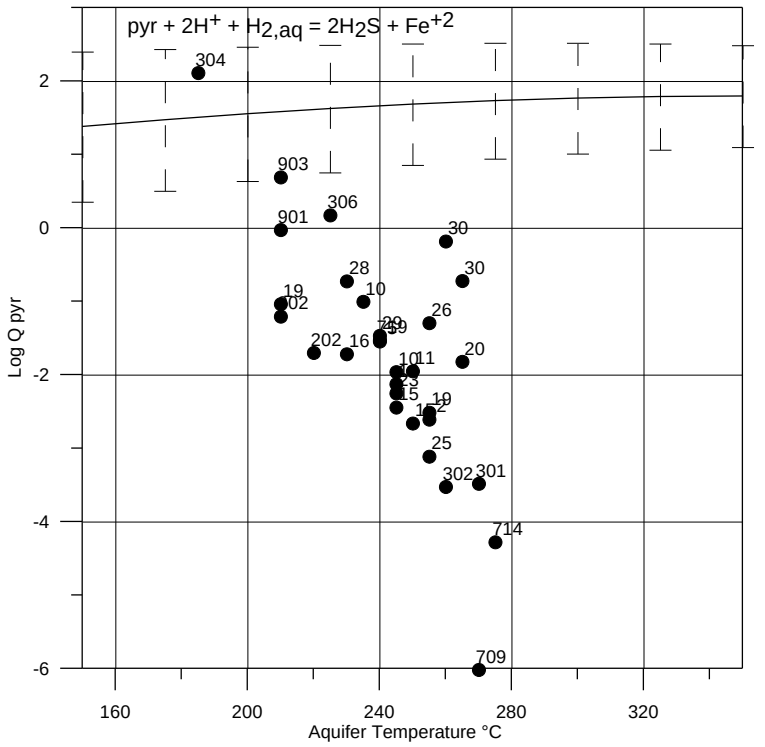

Figure 6.9: Aquifer temperature versus activity product. The continous line depicts the pyrite solubility equilibrium constant dependence with temperature.
Symbols and numbers, see Figure 6.1.

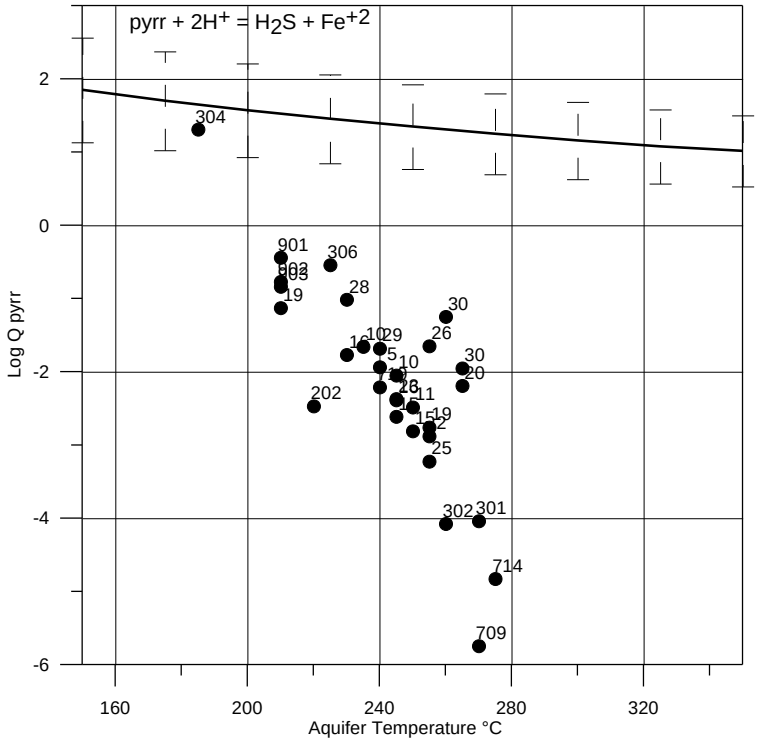

Figure 6.10: Aquifer temperature versus activity product. The continous line depicts the pyrrhotite solubility equilibrium constant dependence with temperature. Symbols and numbers, see Figure 6.1.

A large departure from equilibrium is indicated for both minerals ranging from about saturation to under-saturation by about six log Q units.

The calculated log Q values for both pyrite and pyrrhotite carry much uncertainty because the activities of the Fe^{+2} species are imprecisely evaluated due to inadequate thermodynamic data on ferrous and ferric hydrolysis constants. Also, there is uncertainty involved in calculating the relative abundance of the ferrous and ferric species. For the present study the Fe^{+2}/Fe^{+3} activity ratio was retrieved from analysis of sulphate and sulphide assuming redox equilibrium between these species. Stefánsson and Arnórsson (2002) have demonstrated that such an equilibrium is not very closely approached in high-temperature geothermal systems hosting dilute fluids of meteoric origin. Samples may be contaminated with iron from the casing and surface pipeworks. Finally, iron could have been removed from solution by precipitation as sulphides where extensive boiling occurs by depressurization in producing aquifers and within the wellbore. All these errors and processes make it difficult to confidently assess the state of pyrite and pyrrhotite saturation in the aquifer water.

Arnórsson et al. (2002) have demonstrated that published thermodynamic values for ferrous and ferric hydrolysis constants lead to over-estimation of the $Fe(OH)_4^-$ species activity and a corresponding under-estimation of the activity of the Fe^{+2} species and that the degree of under-estimation of Fe^{+2} activity increases with rising temperature. Calculated Fe^{+2} activities vary by 8 orders of magnitude, Fig 6.11, and there is a good correlation between the calculated activity of Fe^{+2} and the saturaton index for both pyrite and pyrrhotite.

The results in Figure 6.12 indicate that H_{2aq}/H_2S_{aq} activity ratios generally correspond closely to simultaneous equilibrium between solution, pyrite and pyrrhotite. The apparent discrepancy

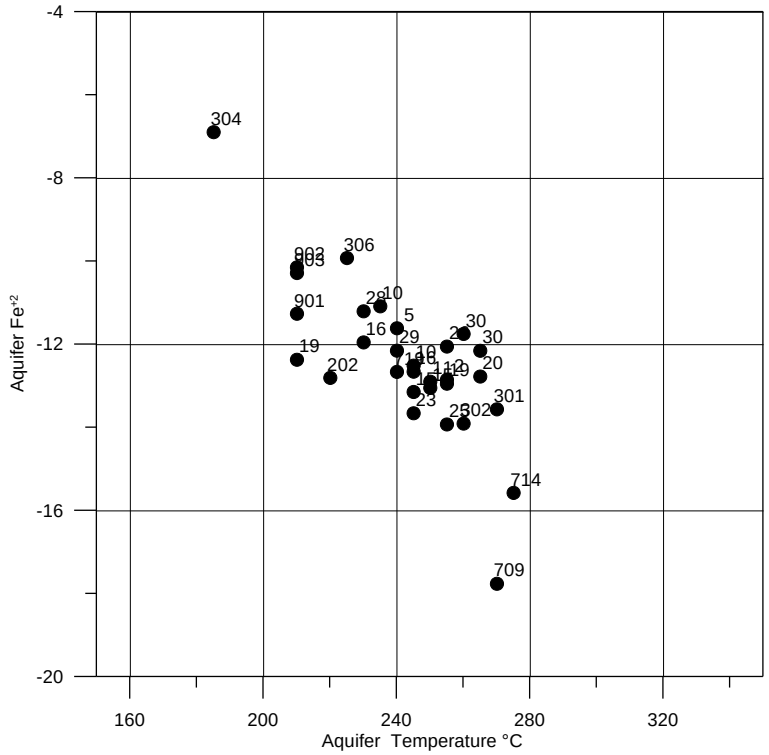

Figure 6.11: Aquifer temperature versus aquifer Fe^{+2}. Symbols and numbers, see Figure 6.1.

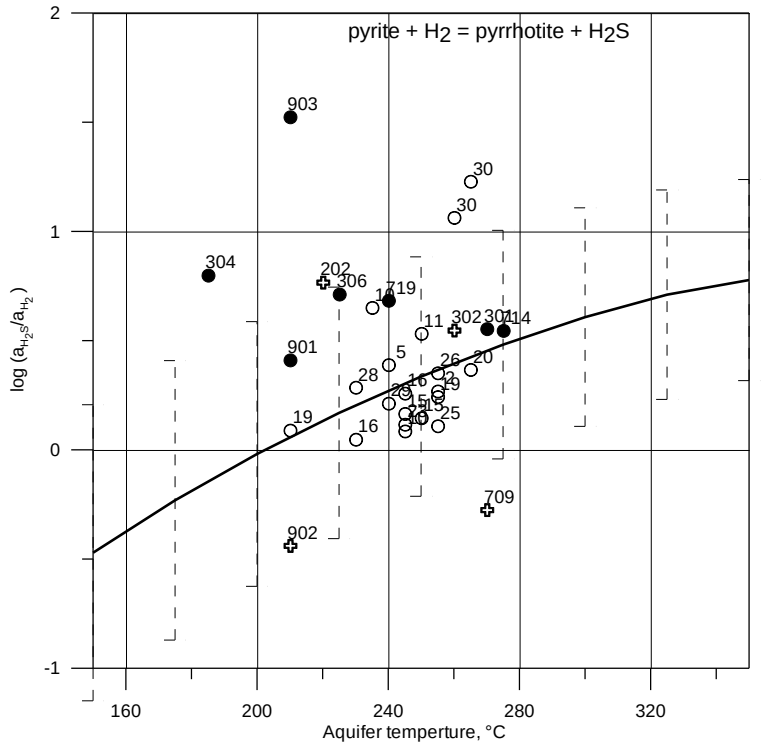

Figure 6.12: Aquifer temperature versus (H_2S/H_2) activity ratio. The continous line depicts the pyrite – pyrrhotite mineral buffer reaction equilibrium constant dependence with temperature. Symbols and numbers, see Figure 6.1.

from equilibrium for the individual minerals is considered to be due to faulty values in calculated Fe^{+2} activities. Contamination, sulphide precipitation and error in calculated aquifer pH may also contribute to the derivation of erroneous Fe^{+2} activities in the aquifer water. In contrast to Fe^{+2}, H_{2aq} and H_2S_{aq} activities in the aquifer water are considered to be relatively accurately evaluated. Yet, atmospheric contamination of steam samples will tend to yield low H_2S concentrations through its oxidation by atmospheric oxygen, and the presence of equilibrium steam will produce high H_2 concentrations. The low H_2S/H_2 ratios for wells 709 and 902 are attributed to atmospheric contamination. The high H_2S/H_2 ratios for wells 903 and 304 are most likely due to the presence of equilibrium steam in the aquifer, which raises the H_2, content of the aquifer fluid.

The data points depicting the state of magnetite saturation in Figure 6.13 show a large scatter around the equilibrium curve from under-saturation by about four orders of magnitude to about equal over-saturation. The largest variation in the log Q value for magnetite is caused by variation in the calculated Fe^{+2} activity. It decreases with rising aquifer temperature by about 8 orders of magnitude. As for pyrite and pyrrhotite, contamination, sulphide precipitation and error in calculated aquifer pH may also contribute to the low SI values derived for magnetite in the aquifer water.

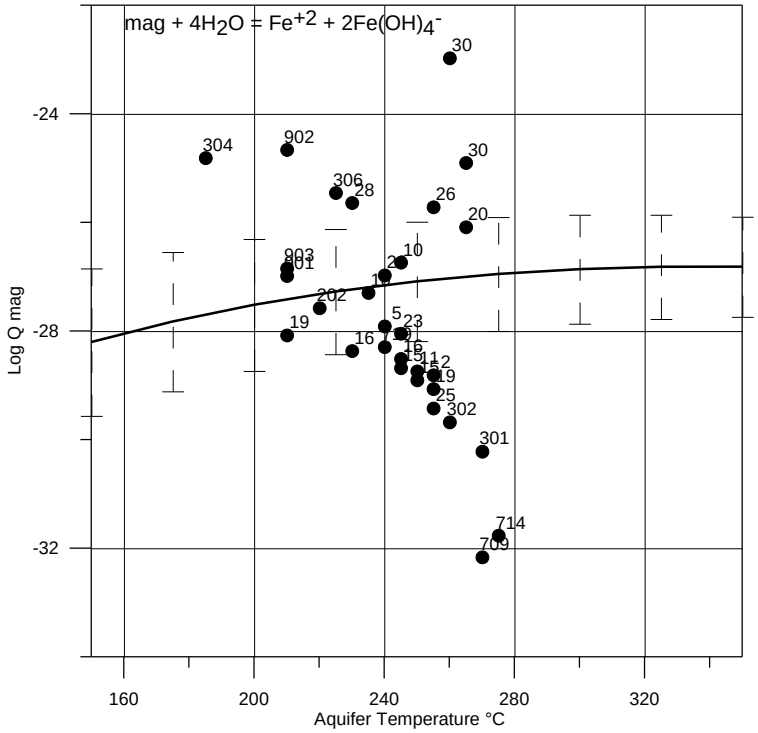

Figure 6.13: Aquifer temperature versus activity product. The continous line depicts the magnetite solubility equilibrium constant dependence with temperature. Symbols and numbers, see Figure 6.1.

The results shown in Figure 6.14 indicate that the aquifer water at Olkaria is close to simultaneous equilibrium with pyrite and magnetite. Only two samples indicate under-saturation. However, the calculated low log Q values for these samples are considered faulty due to low H_2S in the gas samples caused by their atmospheric contamination. As pyrite, pyrrhotite and magnetite are close to being at equilibrium with aqueous H_2S and H_2, this mineral buffer should control both the H_2 and H_2S activity in the aquifer water, as indeed supported by the results of Figures 6.15 and 6.16.

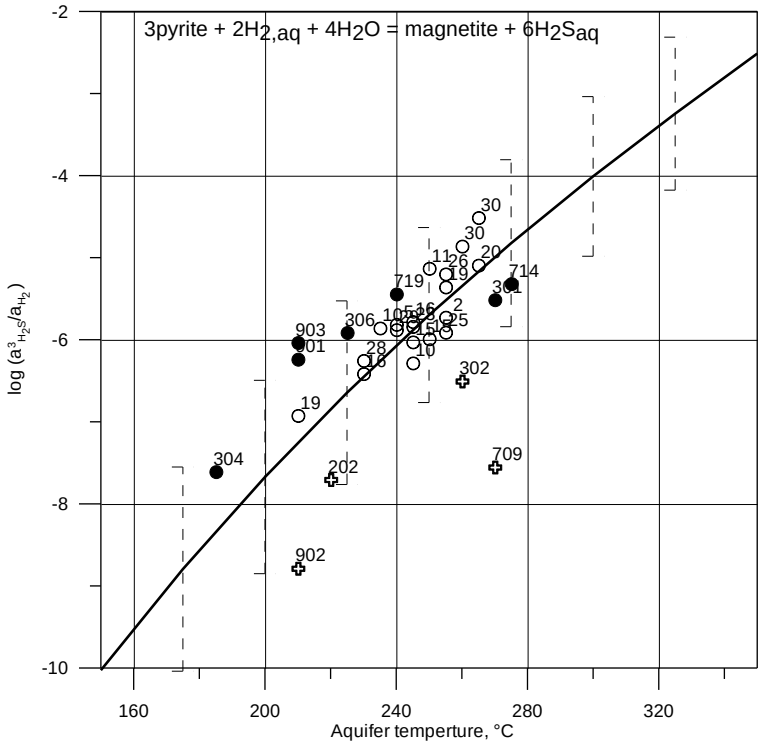

Figure 6.14: Aquifer temperature versus H_2S/H_2 activity ratio. The continous line depicts the pyrite – magnetite equilibrium constant dependence with temperature. Symbols and numbers, see Figure 6.1.

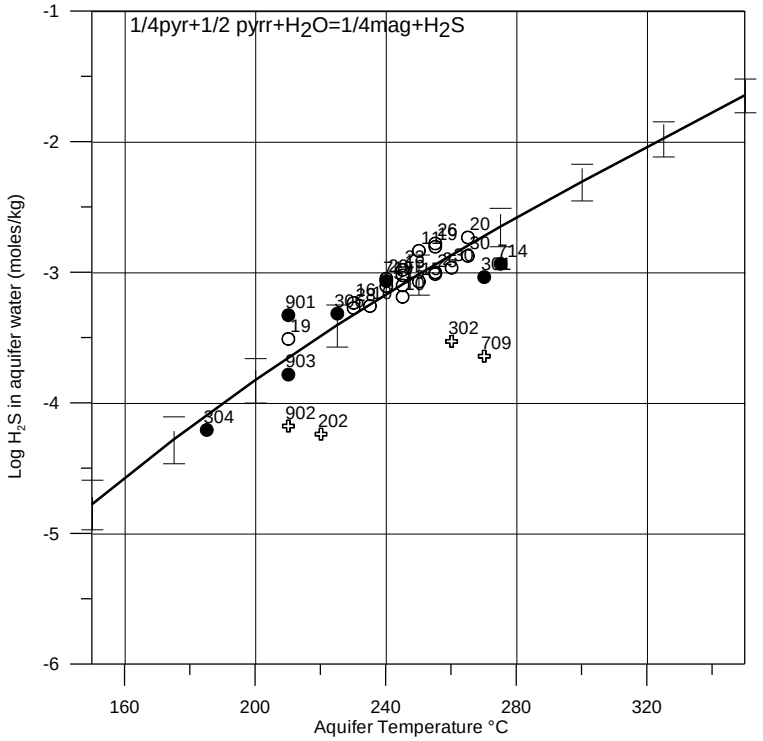

Figure 6.15: Aquifer temperature versus log H_2S in aquifer water. The continous line depicts the pyrrhotite – pyrite – magnetite mineral buffer reaction equilibrium constant dependence with temperature. All the mineral phases have unit activity. Symbols and numbers, see Figure 6.1.

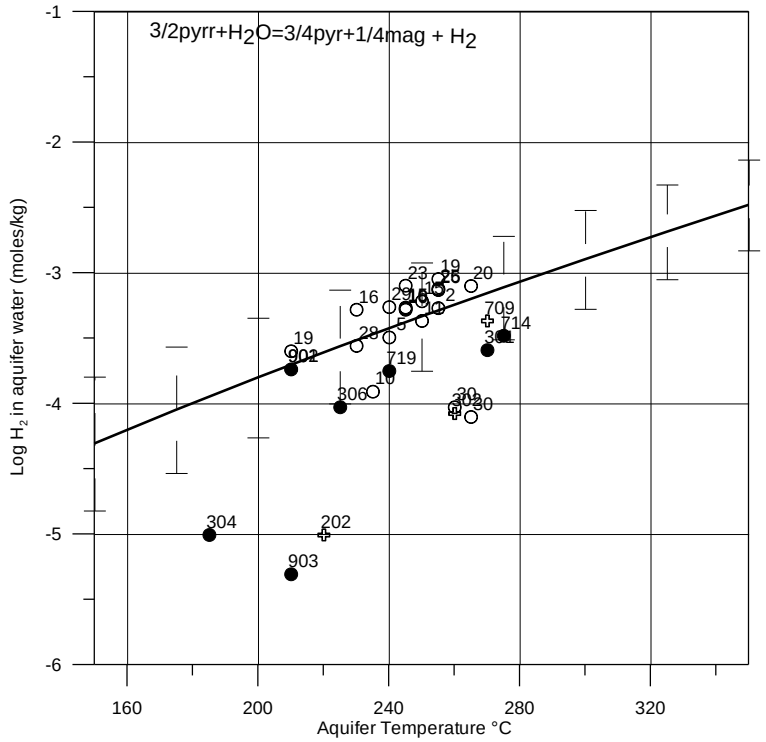

Figure 6.16: Aquifer temperature versus log H_2 in aquifer water. The continous line depicts the pyrrhotite – pyrite – magnetite mineral buffer reaction equilibrium constant dependence with temperature. All the mineral phases have unit activity. Symbols and numbers, see Figure 6.1.

6.6 Wollastonite

Practically all the aquifer waters at Olkaria are significantly wollastonite under-saturated (Figure 6.17). The only water that appears over-saturated is from well OW-709 which is also strongly calcite over-saturated (Figure 6.1). This result is considered faulty due to high measured pH of the water sample collected from the wierbox. It is concluded that wollastonite is not a stable mineral in the Olkaria geothermal reservoir.

6.7 Calcium ion/proton activity ratios

Equilibration of the aquifer water with various mineral buffers could control its $Ca^{+2}/(H^{+})^2$ activity ratio. They include wollastonite-quartz (wol-qtz), prehnite-clinozoisite-quartz (pre-czo-qtz) and grossular-clinozoisite-quartz (gro-czo-qtz). The equilibrium curves for reactions involving these buffers have been plotted in Figures 6.18 – 6.20 along with the respective $Ca^{+2}/(H^{+})^2$ activity ratios of the aquifer water. Almost all samples are, within the limit of error for the equilibrium constant, at equilibrium with prehnite-clinozoisite-quartz and grossular-clinozoisite –quartz buffer but their pH is too low and/or their Ca^{+2} activity too low for equilibrium with the wol-qtz buffer, Fig 6.18. These results are consistent with those for individual minerals discussed above. On average the SI value is +0.06 for the pre-czo-qtz buffer and –0.45 for the gro-czo-qtz buffer, the standard deviations being 0.76 and 0.82, respectively. When considering the errors in the log K values (0.65 and 1.47 for the pre-czo-qtz and gro-czo-qtz buffers, respectively, at 250°C) alone for these two buffers, the difference in the SI values are not sufficiently large to discriminate which of the two buffers could control the $Ca^{+2}/(H^{+})^2$ activity ratios.

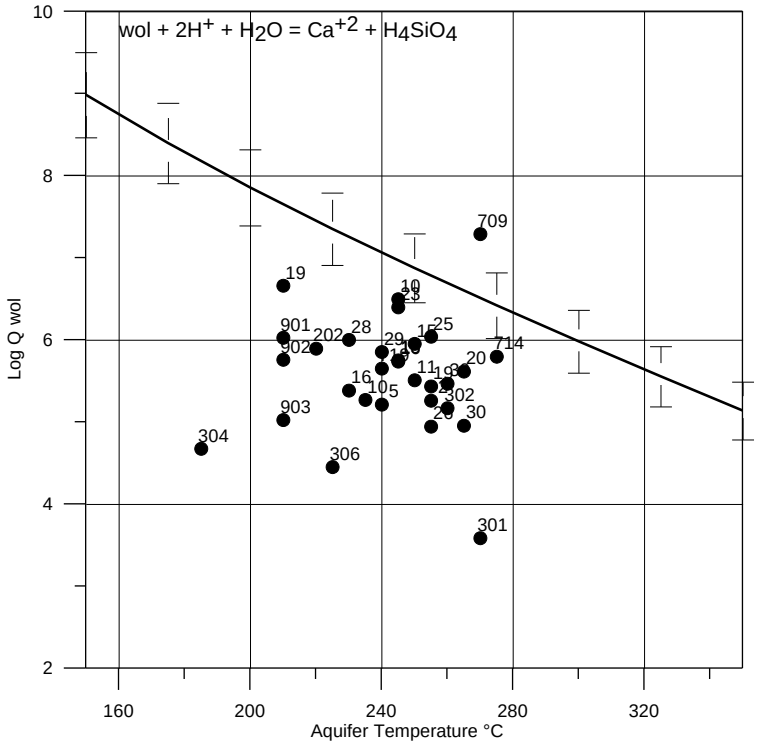

Figure 6.17: Aquifer temperature versus $Ca^{+2}/(H^{+})_2$ activity ratio. The continous line depicts the wollastonite solubility equilibrium constant dependence with temperature. Symbols and numbers, see Figure 6.1.

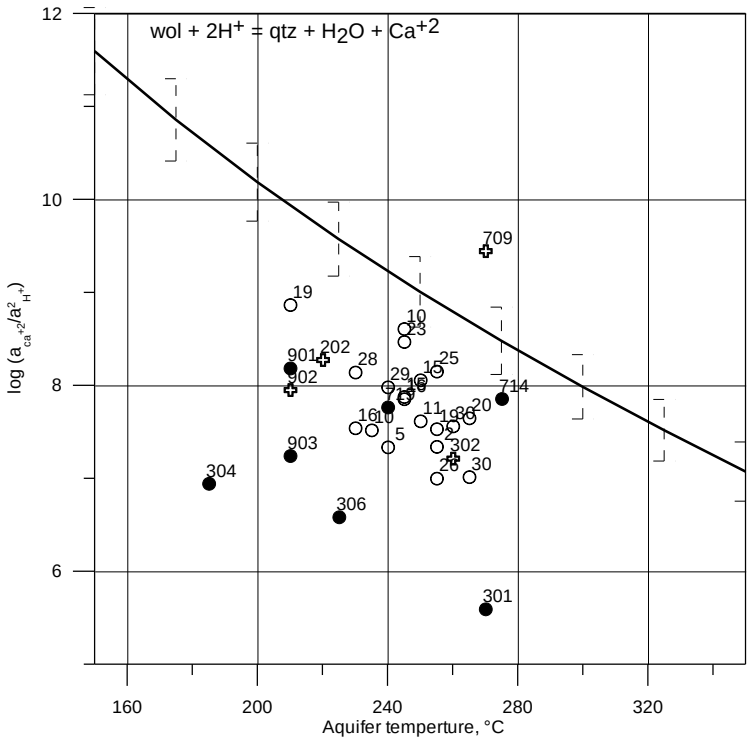

Figure 6.18: Aquifer temperature versus $Ca^{+2}/(H^{+})_2$ activity ratio. The continous line depicts the wollastonite – quartz mineral pair reaction equilibrium constant dependence with temperature. Symbols and numbers, see Figure 6.1.

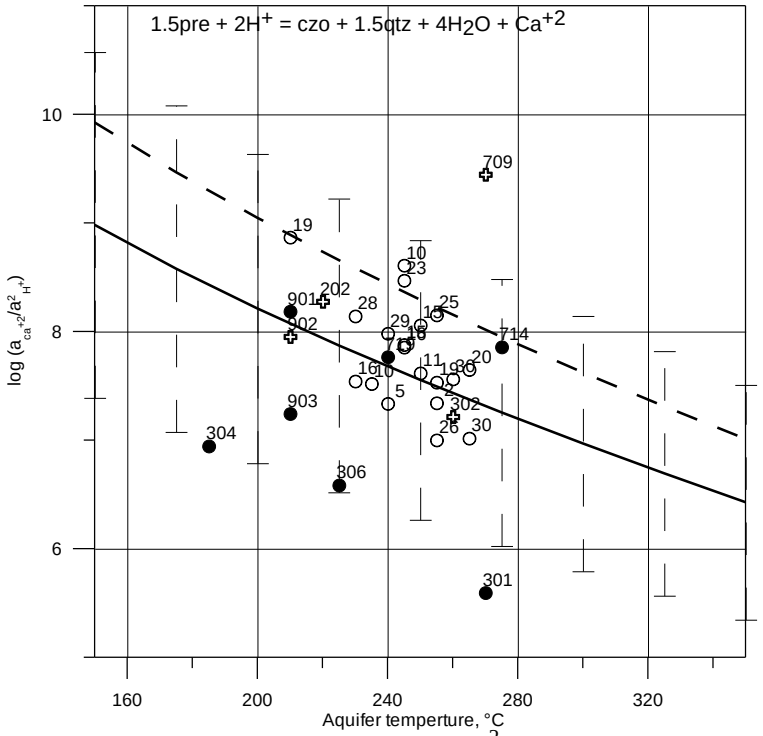

Figure 6.19: Aquifer temperature versus log (a_{Ca+2} / a^2_{H+}) activity ratio. The continous line depicts the prehnite – clinozoisite mineral pair reaction equilibrium constant dependence with aquifer temperature. The activity of the clinozoisite is 0.07 while all the other mineral phases have unit activity. Dotted curve has data for prehnite from Berman (1985). Symbols and numbers, see Figure 6.1.

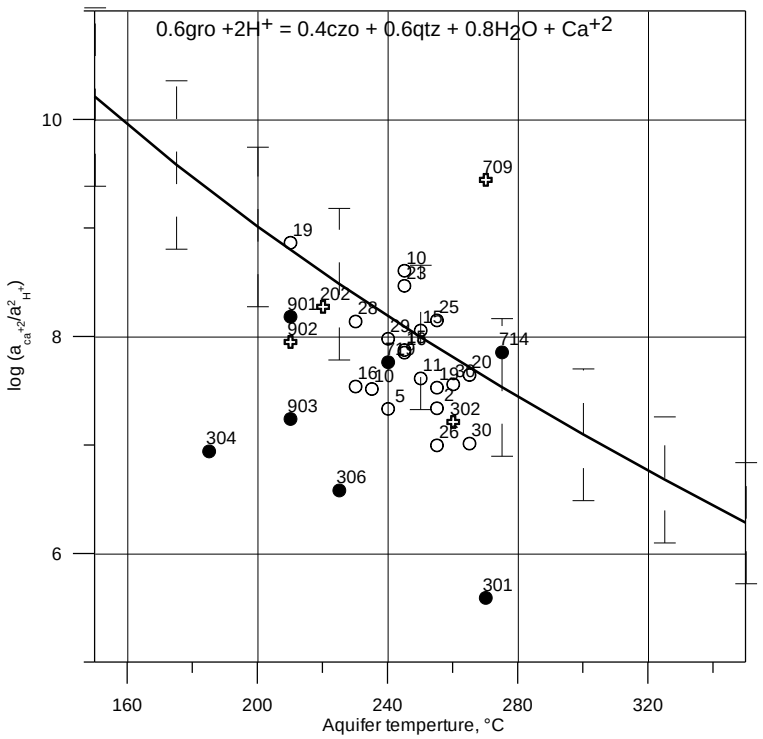

Figure 6.20: Aquifer temperature versus log (a_{Ca+2}/a^2_{H+}). The continous line depicts the grossular – clinozoisite – quartz mineral reaction equilibrium constant dependence with temperature. The activity of the grossular and clinozoisite are taken to be 0.43 and 0.07 respectively, (the average composition of these minerals in the Olkaria geothermal reservoir) while all the other mineral phases have unit activity. Symbols and numbers, see Figure 6.1.

The relatively low $Ca^{+2}/(H^{+})^2$ activity ratios for wells 301, 304, 306 and 903 and low ratio for well 709 can be accounted for by erroneous aquifer pH. These waters also show logQ values that differ much from other samples for the Al-silicates (clinozoisite, epidote, prehnite and grossular) and wollastonite, all of which have pH dependent solubility.

6.8 $Fe(OH)_4^-/OH^-$ activity ratios

The mineral buffers epidote-prehnite (epi-pre) or epidote-grossular-wollastonite-quartz (epi-gro-wol-qtz) could control $Fe(OH)_4^-/OH^-$ activity ratios in the aquifer water. The calculated activity products are compared with the respective equilibrium constants in Figures 6.21 and 6.22. Most of the waters have higher $Fe(OH)_4^-/OH^-$ activity ratios than those corresponding with equilibrium for the mineral buffers in question.

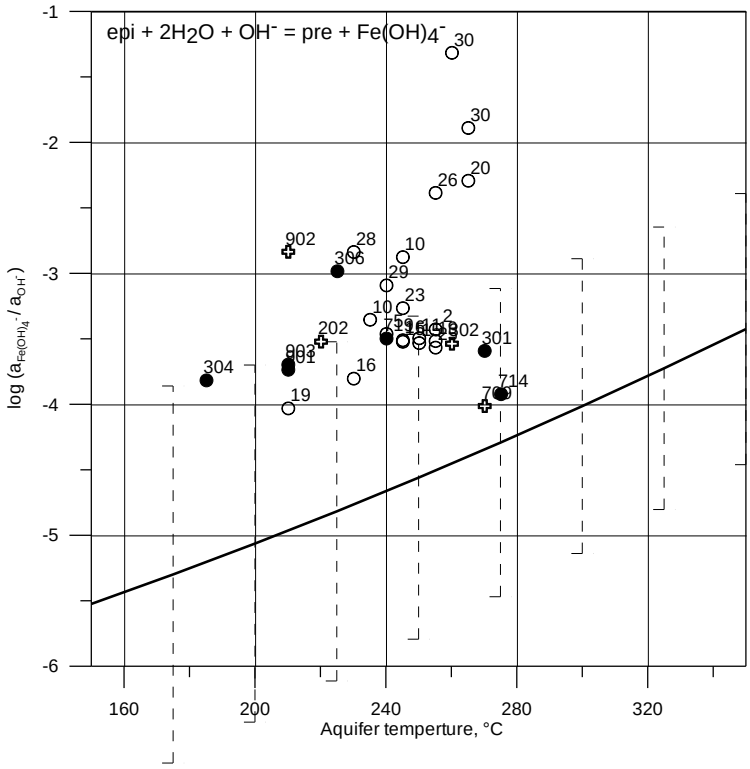

Figure 6.21: Aquifer temperature versus log ($a_{Fe(OH)4-}$ / a_{OH-}) activity ratio. The continous line depicts the epidote – prehnite mineral pair reaction equilibrium constant dependence with aquifer temperature. All the mineral phases have unit activity.
Symbols and numbers, see Figure 6.1.

6.9 Carbon dioxide

It follows from the results that the aquifer water at Olkaria is in equilibrium with calcite (cal) and that the buffer pre-czo-qtz controls $Ca^{+2}/(H^{+})^2$ activity ratios, and that the buffer pre-czo-cal-qtz controls aqueous CO_2 concentrations (CO_2 partial pressures). This is indeed verified by the results depicted in Figure 6.23. The CO_2 concentrations in all aquifer waters are, within the limit of error for log K, at equilibrium with this mineral buffer. Most of the waters, however, have negative SI values, the average being 0.6 SI units. Waters from Olkaria West have high CO_2 aquifer water concentrations and marginal wells tend to be intermediate between Olkaria West and the Olkaria East Field.

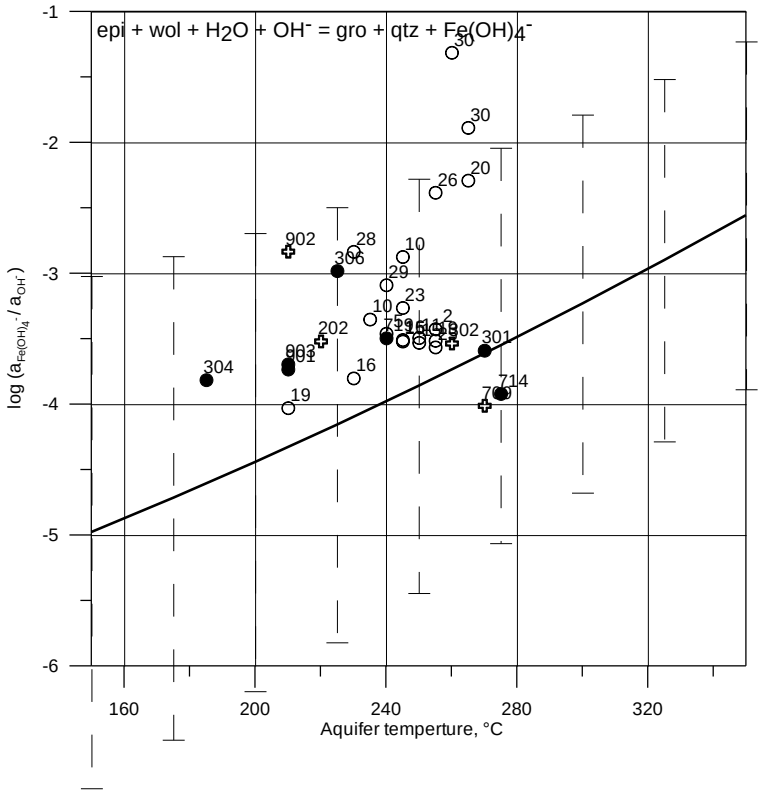

Figure 6.22: Aquifer temperature versus log ($a_{Fe(OH)4-}$ / a_{OH-}) activity ratio. The continous line depicts the epidote – wollastonite – quartz – grossular mineral reaction equilibrium constant dependence with aquifer temperature. The activity of grossular is 0.43 while all the other mineral phases have unit activity. Symbols and numbers, see Figure 6.1.

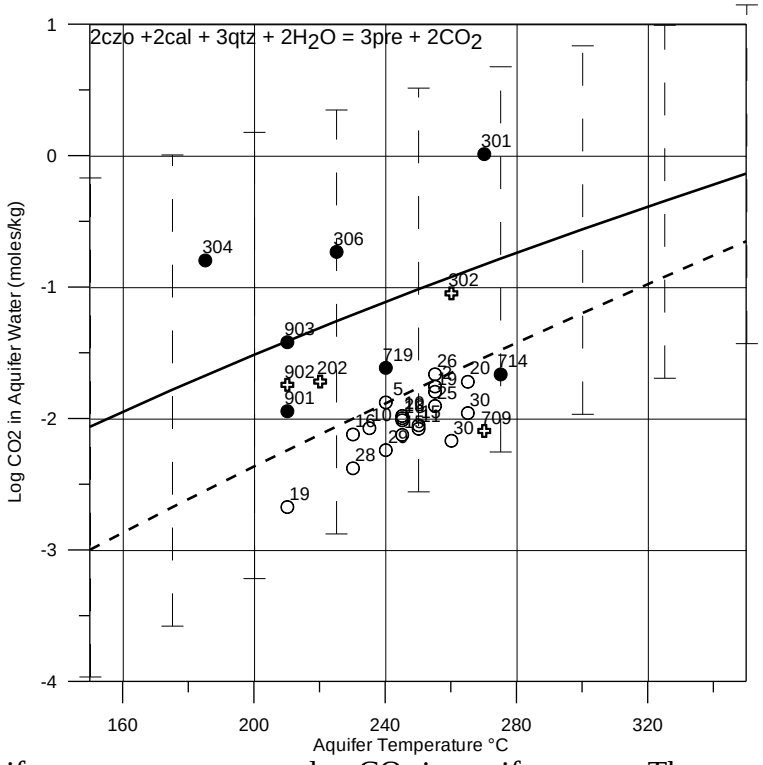

Figure 6.23: Aquifer temperature versus log CO_2 in aquifer water. The continous line depicts the clinozoisite – calcite – quartz – prehnite mineral buffer reaction equilibrium constant dependence with temperature. The dotted line illustrates the same but the data for prehnite is from Berman (1985). The activity of clinozoisite is taken to be 0.07. All the mineral phases have unit activity. Symbols and numbers, see Figure 6.1.

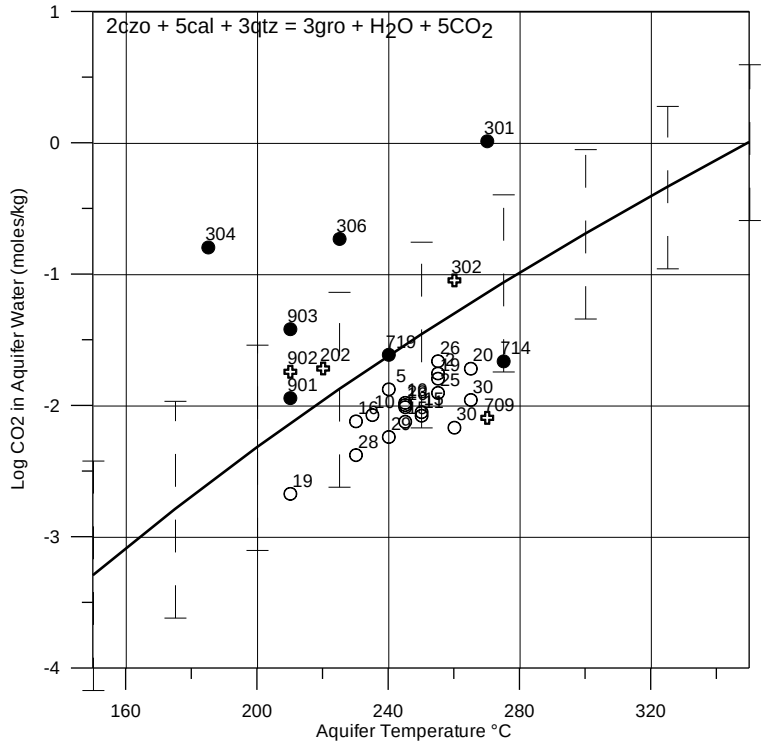

Figure 6.24: Aquifer temperature versus log CO_2 activity ratio. The continous line depicts the clinozoisite – calcite – quartz – grossular mineral buffer reaction equilibrium constant dependence with aquifer temperature. The activity of clinozoisite and grossular is taken to be 0.07 and 0.43 respectively (the average composition of those minerals in the Olkaria geothermal reservoir), while all the other mineral phases have unit activity. Symbols and numbers, see Figure 6.1.

The departure of the data points from the equilibrium curve may be the cause of faulty thermodynamic data on the minerals used to retrieve values for the equilibrium constant. Also the position of the equilibrium curve is very sensitive to small variations in the analysed activity of the clinozoisite. The equilibrium pattern for the buffer czo-cal-qtz-gro is very similar to that for czo-cal-qtz-pre (Figures 6.23 and 6.24). Aqueous CO_2 concentrations would be almost the same at equilibrium with either buffer at a particular temperature.

6.10 Hydrogen and hydrogen sulphide

The calculated concentration of H_2S and H_2 in the aquifer of Olkaria wells corresponds closely to equilibrium with the minerals buffer pyr-pyrr-pre-epi (Figure 6.25 and 6.26). Yet, the calculated aqueous H_2 concentrations tend to be a little high in relation to the equilibrium curve. This may be explained by the presence of a small fraction of equilibrium steam in the aquifer fluids. The presence of such steam would depress the H_2 concentrations in the liquid because of its low solubility in water. The effect on H_2S would be much smaller due to its higher solubility in water. The aquifer water of the marginal wells is a little low in H_2S. The cause could be equilibration with another mineral buffer.

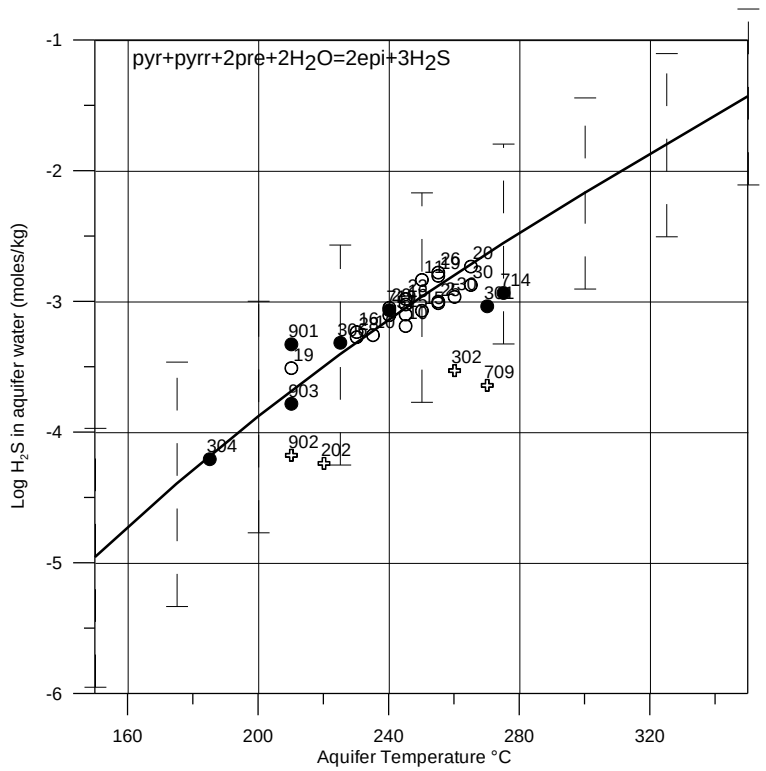

Figure 6.25: Aquifer temperature versus log H_2S in aquifer water. The continous line depicts the pyrrhotite – pyrite – prehnite – epidote mineral buffer reaction equilibrium constant dependence with temperature. All the mineral phases have unit activity.
Symbols and numbers, see Figure 6.1.

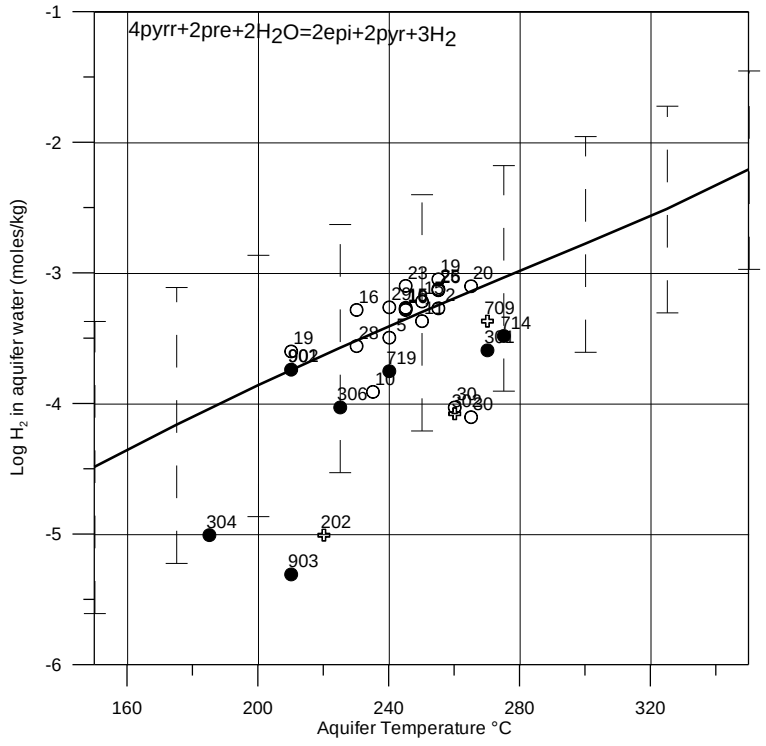

Figure 6.26: Aquifer temperature versus log H_2 in aquifer water. The continous line depicts the pyrrhotite – prehnite – epidote – pyrite mineral buffer reaction equilibrium constant dependence with temperature. All the mineral phases have unit activity.
Symbols and numbers, see Figure 6.1.

Calculated H_2S and H_2 concentrations in the aquifer water are somewhat higher than those predicted by equilibrium with a mineral buffer involving gro-pyr-pyrr-qtz-epi, yet within the limit of error in the calculated logK values (Figures 6.27 and 6.28. The same applies to the buffer which includes magnetite instead of pyrrhotite (Figures 6.29 and 6.30). As for CO_2, different mineral buffers yield similar aqueous H_2S and H_2 concentrations at equilibrium. Thus, when considering the error in the thermodynamic data used to calculate the respective equilibrium constants, it is not possible to predict from data on the geothermal fluid compositions which mineral buffer may control the respective gas concentrations in the aquifer water.

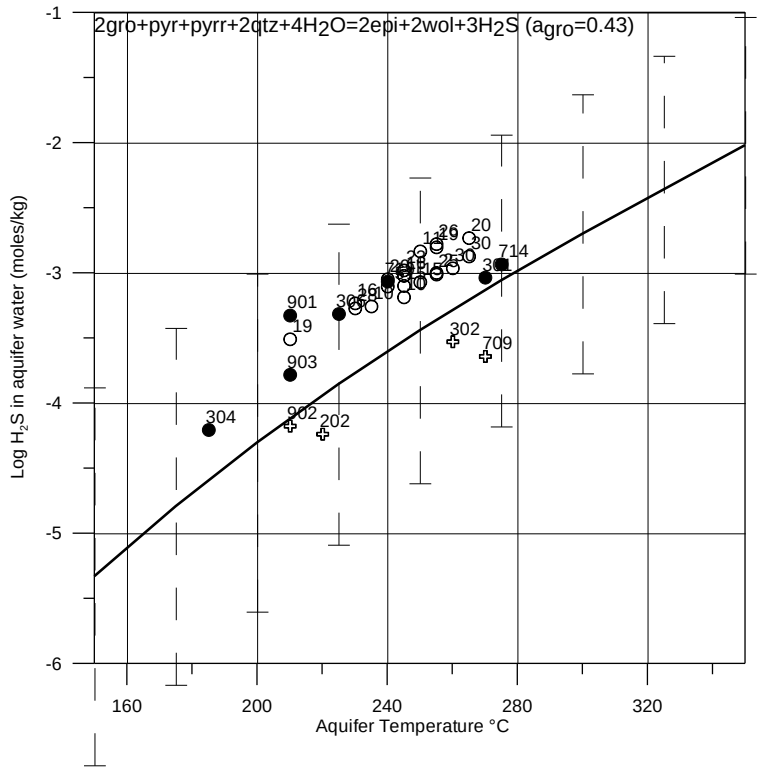

Figure 6.27: Aquifer temperature versus log H_2S in aquifer water. The continous line depicts the grossular – pyrite – pyrrhotite – quartz – epidote – wollastonite mineral buffer reaction equilibrium constant dependence with temperature. The activity of the grossular is taken to be 0.43. All the other mineral phases have unit activity. Symbols and numbers, see Figure 6.1.

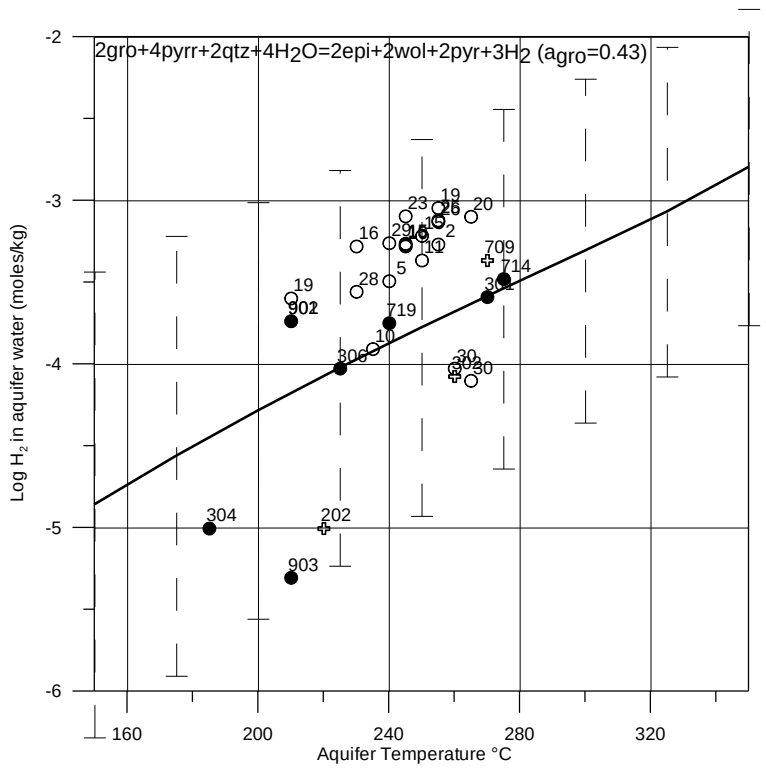

Figure 6.28: Aquifer temperature versus log H_2 in aquifer water. The continous line depicts the grossular - pyrrhotite – quartz – epidote – wollastonite – pyrite mineral buffer reaction equilibrium constant dependence with temperature. The activity of the grossular is taken to be 0.43. All the other mineral phases have unit activity. Symbols and numbers, see Figure 6.1.

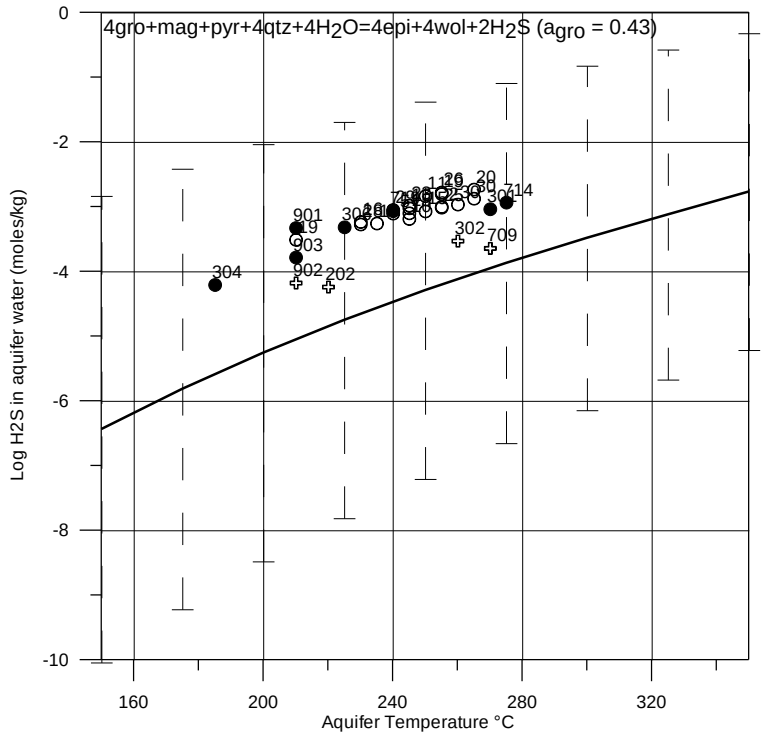

Figure 6.29: Aquifer temperature versus log H_2S in aquifer water. The continous line depicts the grossular – magnetite – pyrite – quartz – epidote – wollastonite mineral buffer reaction equilibrium constant dependence with temperature. The activity of the grossular is taken to be 0.43. All the other mineral phases have unit activity. Symbols and numbers, see Figure 6.1.

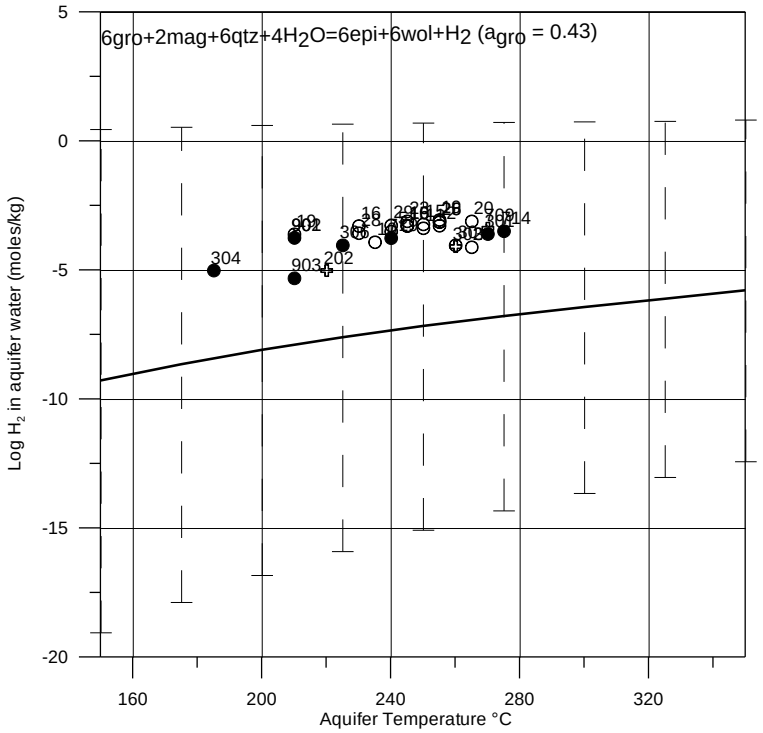

Figure 6.30: Aquifer temperature versus log H_2 in aquifer water. The continous line depicts the grossular – magnetite – quartz – epidote – wollastonite mineral buffer reaction equilibrium constant dependence with temperature. The activity of the grossular is taken to be 0.43. All the other mineral phases have unit activity.
Symbols and numbers, see Figure 6.1.

7.0 DISCUSSION AND CONCLUSIONS

A good linear correlation exists between the saturation indices of clinozoisite, grossular, prehnite and aquifer pH. Multiple linear regression gives a slope of 2 for prehnite and grossular and a slope of 1 for prehnite and clinozoisite. The corresponding correlation coefficients are both 0.9. At a saturation index value (SI) of zero for prehnite the corresponding values are –1.5 and – 2 for clinozoisite and grossular, respectively. This discrepancy cannot be explained by removal of Ca or Al or both from solution between aquifer and wellhead or errors in the selected thermodynamic properties for the aqueous species selected to calculate the respective solubility constants. It must be due to lack of equilibration between solution and one or more of these minerals, or error in the selected values for their thermodynamic properties.

There are difficulties in calculating aquifer fluid compositions from analysis of samples collected at the wellhead, and more so for samples collected for excess enthalpy wells. In this study, the model assumed that excess enthalpy is due to phase segregation and no aquifer steam was present in the producing aquifer. However, it is known that parts of the aquifer are two-phase. If equilibrium steam is truly present, then this model would lead to derivation of activity products for minerals with pH dependent solubility which are too low. Additionally, precipitation of minerals upon extensive boiling of the water will cause wellhead samples to differ in composition from aquifer fluid. All this creates difficulty in assessing the state of mineral saturation in the aquifer water.

Equilibrium constant (K) temperature dependence functions for individual minerals, mineral pairs and mineral buffers were derived from thermodynamic data. Errors associated with the thermodynamic data were retrieved and evaluated. Activity products and or ratios were determined and the respective saturation indices computed. The aquifer waters in the Olkaria geothermal reservoir are at equilibrium or very close to equilibrium with respect to the following minerals; calcite, clinozoisite, epidote and prehnite. Evidence indicates that the aquifer waters are also close to equilibrium with respect to pyrite, pyrrhotite and magnetite.

Thus the H_2S/H_2 activity ratio corresponds closely to equilibrium with the mineral pairs pyrite/pyrrhotite and pyrite/magnetite. However, the present results indicate general under-saturation with respect to the individual minerals. This apparent under-saturation is considered to be the consequence of faulty thermodynamic data on iron (Fe) hydrolysis constants.

The aquifer waters are moderately undersaturated with respect to grossular and wollastonite. The calcium/proton squared $(Ca^{+2}/(H^{+})^2)$ activity ratios of the aquifer waters are on average slightly lower than the equilibrium values for the mineral pair of grossular-clinozoisite but close to equilibrium value for the prehnite-clinozoisite. The aquifer waters have higher $Fe(OH)_4^-/OH^-$ activity ratios than the equilibrium values for the mineral pair epidote-prehnite and the mineral buffer epidote-wollastonite-grossular-quartz. This is probably due to the overestimation of the $Fe(OH)_4^-$ species.

The aquifer fluid is at equilibrium with respect to the mineral pairs of pyrite/pyrrhotite and pyrite/magnetite, with respective saturation indices of 0.16 and 0.006. The activities of aqueous H_2 and H_2S gases generally correspond closely to equilibrium with the mineral buffer pyrite/pyrrhotite/magnetite. Samples showing low H_2 and H_2S values with respect to the equilibrium with the above buffer are from marginal wells whose discharge fluid is mixed

with atmospherically contaminated fluid. The activities of aqueous H_2 and H_2S also correspond closely to equilibrium with the mineral buffer pyrrhotite-prehnite-epidote-pyrite. At present it is not possible to conclusively identify which of the two buffers control the activities of the aqueous H_2 and H_2S. The clinozoisite-calcite-quartz-prehnite buffer is considered to control the CO_2 activity in the aquifer.

REFERENCES

Ambusso, W. J. and Ouma, P. A., (1991): Thermodynamic and permeability structure of Olkaria North East Field: Olkaria fault. *Geothermal Resources Council Transactions* 15, 237-242.

Ármannsson, H., (1996): *Fluid chemistry and utilisation.* UNU G.T.P., Iceland, unpublished lectures from the specialized lecture course.

Ármannsson, H., Gudmundsson, Á., and Steingrímsson, B.S., (1987): Exploration and development of the Krafla geothermal area. *Jökull,* 37, 12-29.

Arnórsson, S., (2000): The quartz and Na/K geothermometers. 1. New thermodynamic calibration. *Proceedings of the World Geothermal Congress 2000, Japan,* 929-934.

Arnórsson, S., and Andrésdóttir, A., (1995): Processes controlling the chemical composition of natural waters I the Hreppar-Land area in southern Iceland. *International Atomic Energy Agency, IAEA TEC-DOC-788,* 21-43.

Arnórsson, S., and Andrésdóttir, A., (1999): The dissociation constants of Al-hydroxy complexes at 0-350°C and Psat. *Proceedings of 5th International Symposium on Geochemistry of the Earth´s Surface (ed. H. Ármannsson),* Rotterdam, Balkema, 425-428.

Arnórsson, S., Björnsson, S., Muna, Z.W., and Bwire Ojiambo, S., (1990): The use of gas chemistry to evaluate boiling processes and initial steam fractions in geothermal reservoirs with an example from the Olkaria field, Kenya. *Geothermics,* 19-6, 497-514.

Arnórsson S., D´Amore F., and Gerardo J. (2000): Isotopic and chemical techniques in geothermal exploration (ed. S. Arnórsson). Vienna, *International Atomic Energy Agency,* 351 pp.

Arnórsson, S., Geirsson, K., Andrésdóttir, A., and Sigurdsson, S., (1996): Compilation and evaluation of thermodynamic data on aqueous species and dissociational equilibria in aqueous solution. I. The solubility of CO_2, H_2S, H_2, CH_4, N_2, O_2 and Ar in pure water. *Science Institute report* 17-96, 20 pp.

Arnórsson, S., and Gunnlaugsson, E., (1985): New gas geothermometers for geothermal exploration - calibration and application. *Geochim. Cosmochim. Acta,* 49, 1307-1325.

Arnórsson, S., Gunnlaugsson, E., and Svavarsson, H., (1983a): The chemistry of geothermal waters in Iceland II. Mineral equilibria and independent variables controlling water compositions. *Geochim. Cosmochim. Acta,* 47, 547-566.

Arnórsson, S., Sigurdsson, S. and Svavarsson, H., (1982): The chemistry of geothermal waters in Iceland I. Calculation of aqueous speciation from 0°C to 370°C. *Geochim. Cosmochim. Acta,* 46, 1513-1532.

Arnórsson, S., and Stefánsson, A., (1999): Assessment of feldspar solubility in water in the range 0-350°C at Psat. *American Journal of Science.*, 299, 173-209.

Berman, R. G., (1988): Internally consistent thermodynamic data for minerals in the system Na_2O-K_2O-CaO-MgO-FeO-Fe_2O_3-Al_2O_3-SiO_2-TiO_2-H_2O-CO_2. *Journal of Petrology,* 29, 455-522.

Bjarnason, J.Ö., (1994): *Speciation program WATCH, ver 2.1.* Orkustofnun, Reykjavík, 7 pp.

Browne P. R. L. (1978): Hydrothermal alteration in active geothermal fields. *Annual Reviews of Earth and Planetary Science* 6, 229-250

Browne P. R. L. (1984): Subsurface stratigraphy and hydrothermal alteration of the easter section of the Olkaria geothermal field, Kenya. *Proceedings of the 6th New Zealand Geothermal Workshop,* Geothermal Institute, Auckland, 33-41.

Castet, S., Dandurand, J. L., Schott, J., and Gout, R., (1993): Boehmite solubility and aqueous aluminium speciation in hydrothermal solutions (90-350°C): Experimental study and modeling. *Geochim. Cosmochim. Acta.,* 57, 4869-4884.

Clarke, G. C., Woodhall, D. G., Allen, D. and Darling, G., (1990): *Geological, Volcanological and Hydrogeological controls on the occurrence of geothermal activity in the area surrounding Lake Naivasha, Kenya.* Ministry of Energy report, Kenya, 245 pp.

Craig, H., 1961: Isotopic variations in meteoric water. *Science,* 133, 1702-1703

Cox, J. D., Wagman, D.D., and Medvedev, V.A., (1989). *CODATA key values for thermodynamics.* Hemisphere Publishing Corp., 271 pp.

Deer, W. A., Howie, R. A., Zussman, J., (1992): *An introduction to the rock-forming minerals*. William Clowes and Sons Ltd., 2nd Edition Appendix 1, 696 pp.

Diakonov, I. I., Schott, J., Martin, F., Harrichourry, J. C., and Escalier, J., (1999a): Iron (III) solubility and speciation in aqueous solutions. Experimental study and modeling: part 1. Hematite solubility from 60 to 300°C in NaOH-NaCl solutions and thermodynamic properties of $Fe(OH)^-_{4(aq)}$. *Geochim. Cosmochim. Acta,* 63, 2247-2261.

Diakonov I. and Tagirov B. R. (2000): Iron (III) speciation in aqueous solutions: Part 2. Thermodynamic properties of $Fe(OH)^{+2}$, $Fe(OH)^{+}_{2}$ and $Fe(OH)^{0}_{3}$ species and solubility of iron (III) oxides and hydroxides. In preparation.

Droop, G. T. R., (1987): A general equation for estimating Fe3+ concentrations in ferromagnesian silicates and oxides from microprobe analyses, using stoichiometric criteria. *Mineralogical Magazine,* September 1987, Vol. 51, pp. 431-5.

Epstein, S., Mayeda, T. (1953): Variation of the 18O contents from natural sources, *Geochim. Cosmochim. Acta,* 4, 213-224.

Fournier, R.O., and Potter, R.W. II, (1982a): A revised and expanded silica (quartz) geothermometer. *Geoth. Res. Council Bull.*, 11-10, 3-12.

Fournier, R.O., and Potter, R.W. II, (1982b): An equation correlating the solubility of quartz in water from 25°C to 900°C at pressures up to 10000 bars. *Geochim. Cosmochim. Acta*, 46, 1969-1974.

Fournier, R.O., and Truesdell, A.H., (1973): An empirical Na-K-Ca geothermometer for natural waters. *Geochim. Cosmochim. Acta*, 37, 1255-1275.

Giggenbach W.F., (1981): Geothermal mineral equilibria. *Geochimica. Cosmochim. Acta* 45, 393-410.

Gottschalk, M., (1997): Internally consistent thermodynamic data for minerals in the system SiO2-TiO2-Al2O3-Fe2O3-CaO-MgO-FeO-K2O-Na2O-H2O-CO2. *European Journal of Mineralogy*, 9, 175-223.

Gudmundsson B. T., and Arnórsson S., (2002): Secondary mineral –fluid equilibria in the Krafla and Námafjall geothermal systems, Iceland. *Applied Geochemistry* (in press).

Gunnarsson I. and Arnórsson S. (2000): Amorphous silica solubility and thermodynamic properties of H4SiO°4 in the range of 0°C to 350°C at Psat. *Geochimica. Cosmochim. Acta* Vol. 64, No. 13, pp. 2295-2307.

Helgeson, H. C. and Kirkham, D. H. (1974): Theoretical prediction of the thermodynamic behavoir of aqueous electrolytes at higher pressures and temperatures. I. Summary of the thermodynamic/electrostatic properties of the solvent. *Amer. J. Sci.*, 274: 1089-1198.

Henley, R.W., Truesdell, A.H., Barton, P.B.Jr., Whitney, J.A., (1984): Fluid – mineral equilibria in hydrothermal systems. *Society of Economic Geologists, Reviews in economic geology*, 1, 267 pp.

Holland, T. J. B., and Powell, R., (1998a): An enlarged and updated internally consistent thermodynamic dataset with uncertainties and correlations: K_2O-Na_2O-CaO-MgO-MnO-FeO-Fe_2O_3-Al_2O_3-TiO_2-SiO_2-C-H_2-O_2: *Journal of metamorphic Petrology*, 8, 89-124.

Holland, T. J. B., and Powell, R., (1998b): An internally consistent thermodynamic data set for phases of petrological interest. *Journal of metamorphic Petrology*, 16, 309-343.

Hovis, G.L., (1988): Enthalpies and volumes related to K-Na mixing and Al-Si order/disorder in alkali-feldspars. *Journal of petrology*, 29, 731-763.

Johnson J.W., Oelkers E.H., and Helgeson H.C., (1992): SUPCRT92: A software package for calculating the standard molal properties of minerals, gases, aqueous species and reactions among them from 1 to 5000 bars and 0 to 1000°C. *Comp. Geosci.* 18, 899-947.

Karingithi, C.W., (1992): *Olkaria East production field geochemical report.* Kenya Power Company ltd., internal report, 96 pp.

Karingithi, C.W., (1993): *Olkaria East production field geochemical report.* Kenya Power Company ltd., internal report, 86 pp.

Karingithi, C.W., (1996): *Olkaria East production field geochemical report.* Kenya Power Company Ltd., internal report, 124 pp.

Karingithi, C.W., (1999): *Olkaria Domes geochemical model.* The Kenya Electricity Generating Company Ltd, internal report, 30 pp.

Karingithi, C.W., (2000): *Geochemical characteristics of the Greater Olkaria geothermal field, Kenya.* Report 9 in: Geothermal Training in Iceland 2000. UNU G.T.P., Iceland, 165-188.

KenGen (1998): *Surface exploration of Kenya's geothermal resources in the Kenya Rift.* The Kenya Electricity Generating Company Ltd, internal report, 84 pp.

KenGen (1999): *Conceptualized model of the Olkaria geothermal field compiled by Muchemi G.G.* The Kenya Electricity Generating Company Ltd, internal report, 46 pp

Kenya Power Company, (1982a): *Programme for geochemical data collection and monitoring of well discharges prepared by Virkir Consulting Group Ltd.*, Kenya Power Company Ltd., internal report, 112 pp.

Kenya Power Company, (1982b): *Status report on steam production, prepared by Merz and McLellan and Virkir Consulting Group Ltd.*, Kenya Power Company Ltd., internal report, 102 pp.

Kenya Power Company, (1984): *Background report for scientific and technical review meeting.* Kenya Power Company Ltd., internal report prepared by KRTA, 254 pp.

Kenya Power Company, (1988): *Report on Olkaria and Eburru geothermal development. Working papers on the North East Olkaria, for STRM,* Kenya Power Company Ltd., internal report, 246 pp.

Kenya Power Company, (1990): *Olkaria West Field information report.* STRM Kenya Power Company Ltd., internal report, 240 pp.

Macdonald R., Davies G. R., Bliss C. M., Leat P. T., Bailey D. K., and Smith R. L., (1987): Geochemistry of high-silica peralkaline rhyolites Naivasha, Kenya Rift Valley. *Journal of petrology,* Vol. 28 part 6, 979-1008.

Leach, T. M. and Muchemi G. G., (1987): Geology and hydrothermal alteration of the North and West exploration wells in the Olkaria geothermal field, Kenya. *Proceedings of the 9th New Zealand Geothermal Workshop,* Geothermal Institute, Auckland, 187-192.

Muchemi, G.G., (1992): *Geology of the Olkaria Northeast field.* Kenya Power Company Ltd., internal report, 27 pp.

Muchemi, G.G., (1993): *Structural map of Olkaria geothermal field showing inferred ring structures.* Kenya Power Company Ltd., internal report.

Muchemi, G.G., (1999): *Conceptualised model of the Olkaria Geothermal Field.* The Kenya Electricity Generating Company Ltd, internal report, 46 pp.

Muna, Z. W., (1982): *Chemistry of well discharges in the Olkaria geothermal field, Kenya*. UNU Geothermal Training Programme, Iceland, Report 8, 38 pp.

Muna, Z. W., (1990): *Overview of the geochemistry of the Olkaria West geothermal field, Kenya.* Kenya Power Company Ltd., internal report, 56 pp.

Mungania, J., (1992): *Geology of the Olkaria geothermal complex.* Kenya Power Company Ltd, internal report 38 pp.

Mwangi, M.N., (2000): Country update report for Kenya 1995-1999. *Proceedings of the World Geothermal Congress 2000,* Japan, 327-335.

Ofwona, C.O., 2002: *A reservoir study of Olkaria East geothermal system, Kenya.* University of Iceland, M.Sc. thesis, UNU Geothermal Training Programme, Iceland, Report 2, 74 pp.

Omenda, P.A., (1992): The Geology of Olkaria well OW-27. Kenya Power Company Ltd., internal report, 22 pp.

Omenda, P.A., (1994): The Geological structure of Olkaria West geothermal field, Kenya. *Stanford Geothermal Reservoir Engineering Workshop,* 19, 125-130.

Omenda, P. A., (1998): The geology and structural controls of the Olkaria geothermal system, Kenya. *Geothermics*, Vol. 27,1, 55-74.

Omenda, P. A., Onacha, S. A. and Ambusso, W. J., (1993): Geological setting and characteristics of the high temperature geothermal systems in Kenya. *Proceedings of the 15th New Zealand Geothermal Workshop, Geothermal Institute, Auckland,* 161-167.

Ouma, P. A., (1999): *Reservoir Engineering Report for Olkaria Domes Field.* Kenya Electricity Generating Company Ltd., internal report, 54 pp.

Palandri J.L. and Reed M.H. (2000): Determination of in situ composition of sedimentary formation waters. *Geochim. Cosmochim. Acta,* in press.

Pokrovskii, V.A., and Helgeson, H.C., (1995): Thermodynamic properties of aqueous species and solubilities of minerals at high pressures and temperatures: the system Al_2O_3-H_2O-NaCl. *American Journal of Science*, 295, 1255-1342.

Pokrovskii, G. S., Schott, J., Salvi, S., Gout, R., and Kubicki, J. D., (1998): Structure and stability of aluminium-silica complexes in neutral to basic solution, Experimental study and molecular orbital calculations. *Mineralogical Magazine,* 62A, 1194-1195.

Plummer, L.N., and Busenberg, E., (1982): The solubilities of calcite, aragonite and vaterite in CO_2-H_2O solutions between 0 and 90°C, and evaluation of the aqueous model for the system $CaCO_3$-CO_2-H_2O. *Geochim. Cosmochim. Acta*, 46, 1011-1040.

Riaroh, D. and Okoth, W., (1994): The geothermal fields of the Kenya rift. *Tectonophysics* 236,117-130.

Simiyu, S.M., Mboya, T.K., Oduong, E.O., and Vyele, H.I., (1997): *Seismic monitoring of the Olkaria Geothermal Area, Kenya.* The Kenya Electricity Generating Company Ltd, internal report, 62 pp.

Smelik E.A., Franz G. and Navrotsky A., (2001): A calorimetric study of zoisite and

clinozoisite solid solutions. *American Mineralogist,* Vol. 86, 80-91.

Stefánsson, A., and Arnórsson, S., (2000): Feldspar saturation state in natural waters. *Geochim. Cosmochim. Acta,* 64,15, 2567-2584.

Strecker, M.R., Blisniuk, P.M., and Eisbacher, G.H. (1990): Rotation of Extension Direction in the Central Kenya Rift, *Geology,* 18, 299 pp.

Robie R.A and Hemingway B.S. (1995): Thermodynamic properties of minerals and related substances at 298.15 K and 1 bar (10^5 Pascals) pressure and at higher temperatures. *U.S.Geological Survey Bull*. 2131, 461 pp.

Wambugu, J.M., (1995): *Geochemical update of Olkaria West geothermal field.* Kenya Power Company Ltd., internal report, 40 pp.

Wambugu, J.M., (1996): Assessment of Olkaria-Northeast geothermal reservoir, Kenya based on well discharge chemistry. Report 20 in: *Geothermal Training in Iceland 1996*. UNU G.T.P., Iceland, 481-509.

Table 1. Chemical analysis results of weirbox water samples and steam samples, from selected Olkaria geothermal wells, the gas concentration is in mmoles/mole of steam

		----------Water sample----------																----------Steam sample----------					
Well	Date	GSP bars	WHP bars	Enth kJ/kg	CO_2	H_2S	B	SiO_2	Na	K mg/kg	Mg	Ca	F	Cl	SO_4	Al	Fe	pH	CO_2	H_2S	H_2	CH_4	N_2	O_2
OW-02	31.01.01	4.8	5.8	1839	74	1.02	6.8	643	557	92	0.01	0.73	69	764	28	0.664	0.02	9.07	1.82	0.101	0.053	0.013	0.035	0.000
OW-05	31.01.01	4.8	5.5	2599	73	1.19	8.7	624	668	102	0.01	1.08	71	933	70	1.105	0.03	8.75	1.82	0.101	0.042	0.002	0.041	0.000
OW-10	31.01.01	4.8	6.0	2730	78	0.17	12.9	773	805	144	0.05	2.46	76	1190	61	0.829	0.05	8.57	1.27	0.078	0.018	0.026	0.090	0.000
OW-11	31.01.01	5.0	5.1	1894	69	0.34	5.7	597	497	81	0.00	0.58	64	696	21	0.698	0.02	8.94	0.96	0.167	0.047	0.011	0.031	0.000
OW-15	31.01.01	4.5	5.0	2140	92	9.86	5.9	576	526	83	0.01	0.56	57	658	54	0.787	0.02	9.43	0.99	0.098	0.064	0.008	0.051	0.000
OW-16	31.01.01	4.8	6.0	1534	97	7.14	4.9	502	503	67	0.03	0.35	64	586	44	0.491	0.01	9.37	1.23	0.087	0.077	0.005	0.111	0.000
OW-19	31.01.01	5.2	5.5	2684	126	22.10	4.6	548	425	54	0.04	0.49	70	392	57	0.913	0.02	9.51	1.06	0.104	0.067	0.007	0.098	0.000
OW-20	31.01.01	5.4	5.5	2541	110	1.19	14.3	778	610	97	0.05	0.92	95	822	22	0.432	0.38	8.98	1.82	0.168	0.072	0.006	0.023	0.000
OW-26	31.01.01	7.2	7.5	1881	104	13.60	2.2	657	336	51	0.04	0.24	68	309	24	0.928	0.25	9.39	2.33	0.166	0.076	0.004	0.060	0.000
OW-28	01.02.01	2.1	8.0	2446	72	4.59	6.2	625	441	61	0.01	1.33	50	478	104	0.861	0.12	9.27	0.75	0.088	0.042	0.001	0.036	0.000
OW-29	01.02.01	2.1	8.5	2158	82	3.91	10.1	609	417	63	0.03	0.75	84	509	30	0.669	0.06	8.87	0.81	0.120	0.068	0.001	0.060	0.000
OW-30i	01.02.01	2.1	8.0	2196	48	1.03	3.9	768	406	71	0.03	0.27	52	527	50	1.600	0.91	8.60	0.99	0.119	0.007	0.000	0.046	0.000
OW-30ii	01.02.01	2.1	8.0	2196	61	0.68	3.8	701	394	70	0.04	0.36	53	545	40	1.547	3.37	8.96	0.67	0.107	0.009	0.000	0.066	0.000
OW-10	Jun 1999	4.5	5.0	2535	114	0.91	8.0	638	855	130	0.18	3.91	81	1080	57	0.985	0.10	8.75	1.42	0.079	0.064	0.011	0.062	0.013
OW-15	Jun 1999	4.6	5.6	1899	72	2.60	8.7	604	709	115	0.04	1.67	62	1040	41	0.824	0.02	8.69	1.03	0.096	0.065	0.004	0.065	0.001
OW-16	Jun 1999	4.7	5.9	1384	83	2.06	5.4	573	482	69	0.05	1.01	70	636	36	0.686	0.02	8.97	1.11	0.112	0.057	0.004	0.029	0.000
OW-19	Jun 1999	4.6	5.3	1823	65	9.48	8.9	622	527	94	0.03	1.08	63	700	39	1.048	0.02	9.10	1.65	0.155	0.089	0.007	0.066	0.002
OW-23	Jun 1999	5.0	6.1	2191	132	7.88	4.0	653	370	52	0.05	0.90	75	221	42	0.710	0.04	9.44	1.46	0.131	0.095	0.003	0.045	0.001
OW-25	Jun 1999	4.9	6.4	2516	150	2.12	5.5	641	522	94	0.11	1.20	70	671	28	0.511	0.02	9.15	1.41	0.101	0.078	0.003	0.044	0.001
OW-202	Jun 1999	1.5	5.2	1104	1246	2.38	2.5	320	743	128	0.04	0.79	53	354	75	0.858	0.02	9.30	2.80	0.010	0.000	0.005	0.016	0.001
OW-301	Jun 1999	1.5	7.4	1653	2465	3.96	6.8	855	1283	208	0.07	0.66	105	240	112	0.666	0.02	8.67	76.75	0.064	0.019	0.015	0.203	0.000
OW-302	Jun 1999	1.8	5.7	1234	578	3.43	3.5	744	633	101	0.08	1.04	77	505	54	0.784	0.02	9.72	6.62	0.020	0.006	0.007	0.058	0.009
OW-304D	Jun 1999	2.6	3.9	1672	1752	0.97	3.3	364	959	74	1.73	3.48	24	52	93	0.521	0.14	8.13	206.50	0.048	0.017	0.031	0.313	0.000
OW-306	Jun 1999	1.8	4.0	1037	1081	2.90	6.3	551	850	96	0.08	1.20	62	251	50	1.375	0.09	9.15	20.48	0.052	0.010	0.017	0.141	0.000
OW-709	Jun 1999	1.9	7.1	1921	318	6.54	5.1	649	846	218	0.04	1.41	28	770	73	0.892	0.02	9.93	1.01	0.026	0.034	0.005	0.055	0.000
OW-714	Jun 1999	2.8	14.9	1303	135	8.44	3.6	739	557	108	0.06	0.88	66	682	35	1.053	0.01	9.54	1.46	0.079	0.022	0.006	0.061	0.000
OW-719	Jun 1999	2.9	8.0	1259	162	4.46	4.8	588	536	81	0.04	1.09	46	544	83	1.511	0.02	9.38	2.80	0.096	0.019	0.008	0.074	0.000
OW-901	Jun 1999	1.6	4.3	1854	566	18.30	2.4	529	506	57	0.03	0.72	80	280	124	0.683	0.03	9.80	3.36	0.089	0.044	0.006	0.093	0.002
OW-902	Jun 1999	1.0	3.2	1108	434	2.00	1.5	477	448	41	0.05	1.31	52	212	100	2.117	0.08	9.55	3.22	0.009	0.001	0.014	0.244	0.006
OW-903	Jun 1999	1.3	4.0	953	634	3.51	1.1	443	493	47	0.04	0.71	46	178	103	1.224	0.02	9.43	5.01	0.019	0.004	0.013	0.342	0.012

Table 2. Geothermal wells whose recovered rock cuttings were selected for microprobe analysis

Well	Field	Depths (m)
OW-901	Olkaria Domes	1192-1194, 1626-1630, 1670-1672, 1584-1586, 1602-1604
OW-902	Olkaria Domes	1384-1388, 1392-1396, 1948-1954, 1956-1958
OW-903	Olkaria Domes	1310-1312, 1314-1316, 1940-1942, 2016-2018
OW-5	Olkaria East	1580-1582, 1626-1630, 1750-1754
OW-19	Olkaria East	1906-1908
OW-28	Olkaria East	1448-1450, 1504-1508, 1538-1540
OW-33	Olkaria East	1414-1416, 1606-1608
OW-34	Olkaria East	1540-1542, 1630-1632, 1700-1702

Table 3. Epidote and Garnet solid solutions chemical formulae

EPIDOTE SOLID SOLUTION CHEMICAL FORMULAE

Well	Chemical Formulae	Ca	Fe	Al	Si
OW-05	$Ca_{1.94}Fe_{1.07}Al_{1.93}Si_{3.01}O_{12}(OH)$	1.94	1.07	1.93	3.01
OW-19	$Ca_{1.99}Fe_{1.11}Al_{1.92}Si_{2.98}O_{12}(OH)$	1.99	1.11	1.92	2.98
OW-28	$Ca_{2.01}Fe_{0.79}Al_{2.34}Si_{2.90}O_{12}(OH)$	2.01	0.79	2.34	2.90
OW-33	$Ca_{1.96}Fe_{0.92}Al_{2.16}Si_{2.95}O_{12}(OH)$	1.96	0.92	2.16	2.95
OW-34	$Ca_{1.92}Fe_{0.81}Al_{2.26}Si_{2.94}O_{12}(OH)$	1.92	0.81	2.26	2.94
OW-901	$Ca_{2.05}Fe_{0.88}Al_{2.09}Si_{2.97}O_{12}(OH)$	2.05	0.88	2.09	2.97
Average		1.98	0.93	2.12	2.96
Average STD Dev		0.041	0.117	0.134	0.026

GARNET SOLID SOLUTION CHEMICAL FORMULAE

Well	Chemical Formulae	Ca	Fe	Al	Si
OW-05	$Ca_{2.95}Fe_{1.29}Al_{0.73}Si_{2.94}O_{12}$	2.95	1.29	0.73	2.94
OW-19	$Ca_{2.97}Fe_{1.16}Al_{0.82}Si_{2.99}O_{12}$	2.97	1.16	0.82	2.99
OW-28	$Ca_{3.09}Fe_{1.25}Al_{0.79}Si_{2.88}O_{12}$	3.09	1.25	0.79	2.88
OW-33	$Ca_{3.03}Fe_{1.01}Al_{1.06}Si_{2.89}O_{12}$	3.03	1.01	1.06	2.89
OW-34	$Ca_{2.96}Fe_{1.13}Al_{0.97}Si_{2.89}O_{12}$	2.96	1.13	0.97	2.89
OW-903	$Ca_{2.88}Fe_{1.30}Al_{0.88}Si_{2.66}O_{12}$	2.88	1.30	0.88	2.66
OW-902	$Ca_{3.01}Fe_{1.20}Al_{1.07}Si_{2.84}O_{12}$	3.01	1.20	1.07	2.84
OW-901	$Ca_{2.98}Fe_{1.20}Al_{0.84}Si_{2.91}O_{12}$	2.98	1.20	0.84	2.91
Average		2.98	1.19	0.89	2.87
Average STD Dev		0.041	0.065	0.06	0.038

Table 4. Thermodynamic properties of selected secondary end-member minerals at Olkaria geothermal system at 25°C and 1 bar[a]

Mineral	Formula	ΔG_f°	ΔH_f°	S°	V°	$C_p^\circ = a + bT + c/T^2 + d/T^{0.5} + e/T^3 + fT^2$					
		J/mol	J/mol	J/mol/K	J/bar	a	b $\cdot 10^3$	c $\cdot 10^{-5}$	f $\cdot 10^6$	d	e $\cdot 10^{-6}$
Calcite	$CaCO_3$	-1128500	-1207400	91.710	3.69	99.72	26.92	-21.58			
Clinozoisite	$Ca_2Al_3Si_3O_{12}(OH)$	-6487370[d]	-6882500[b]	301.00[c]	13.63[c]	567.0[c]	18.1[c]	-70.34[c]		-2603[c]	
Epidote	$Ca_2FeAl_2Si_3O_{12}(OH)$	-6075110[d]	-6461900[b]	328.00[c]	13.91[c]	544.60[c]	24.78[c]	-112.30[c]		-1192[c]	
Grossular	$Ca_3Al_2Si_3O_{12}$	-6278500	-6640000	260.12	12.53	1529.3	-699.0	74.43	253.0	-18940	
Magnetite	Fe_3O_4	-1012700	-1115700	146.14	4.45	2659.11	-2521.5	207.34	1367.70	-36455	
Prehnite	$Ca_2Al_2Si_3O_{10}(OH)_2$	-5824700	-6202600	292.80	14.11	946.00	-115.06	27.55		-10560	
Pyrite	FeS_2	-160100	-171500	52.90	2.39	-20.32	50.30	-32.00		1787	
Pyrrhotite	FeS	-101300	-101000	60.30	1.82	50.49					
Quartz	SiO_2	-856300	-910700	41.46	2.27	81.14	18.28	-1.81	5.41	-699	
Water	H_2O	-237140[e]	-285830[e]	69.95[e]		75.59[f]			-3.58[f]		
Wollastonite	$CaSiO_3$	-1549000	-1634800	81.69	3.99	200.78	-25.89	-1.58	7.43	-1826	

[a]If not otherwise specified the data have been taken from Robie and Hemingway (1995). [b]Smelik et al., (2001), [c]Holland and Powell (1998a & b),
[d]Calculated from the reported enthalpy and entropy values used the absolute entropies for the elements given in CODATA (www.codata.org)
[e]Helgeson and Kirkham (1974), [f]Arnórsson and Andrésdottir (1999), consistent with Helgeson and Kirkham (1974).

Table 5. Temperature equations, for the equilibrium constant for individual minerals reactions. They are valid in the range 0-350°C at $P_{sat.}$

Species ratios/products	Reaction	Log K (T)
1.	$cal = Ca^{+2} + CO_3^{-2}$	10.22 - 0.0349*T - 2476/T
2.	$czo + 12H_2O = 2Ca^{+2} + 3Al(OH)_4^- + 3H_4SiO_4 + OH^-$	-716.103 + 12331.29/T –0.20871 T + 281.836 log T
3.	$ep + 12H_2O = 2Ca^{+2} + Fe(OH)_4^- + 2Al(OH)_4^- + 3H_4SiO_4 + OH^-$	-659.533 + 9484.71/T – 0.18697 T +256.795 log T
4.	$gro + 4H^+ + 8H_2O = 3Ca^{+2} + 2Al(OH)_4^- + 3H_4SiO_4$	-610.614 + 21310.18/T – 0.16166 T + 238.878 log T
5.	$mag + 4H_2O = 2Fe(OH)_4^- + Fe^{+2}$	-140.944 – 218.63/T –0.03477 T + 48.723 log T
6.	$pre + 10H_2O = 2Ca^{+2} + 2Al(OH)_4^- + 2OH^- + 3H_4SiO_4$	-688.574 + 10205.56/T –0.208095 T + 272.716 log T
7.	$pyr + 2H^+ + H_2,aq = 2H_2S + Fe^{+2}$	-94.135 + 2870.58/T – 0.017784 T + 36.647 log T
8.	$pyrr + 2H^+ = H_2S + Fe^{+2}$	-27.885 + 2496.81/T – 0.00249 T + 9.470 log T
9.	$wol + 2H^+ + H_2O = Ca^{+2} + H_4SiO_4$	-45.937 + 5440.14/T -0.01353 T + 18.191 log T

Table 6. Mineral pairs reactions controlling calcium/proton (a_{Ca+2}/a_{H+}) and hydrogen sulphide/hydrogen (a_{H2S} / a_{H2}) activity ratio in solution and respective log K temperature equations

Species activity ratios		Reaction	Log K (T)
1.	$a_{Ca^{+2}}/a_{H^+}^2$	$3gro + 10H^+ = 4H_2O + 2czo + 3qtz + 5Ca^{+2}$	-22.967 + 4977.28/T - 0.008579*T + 9.526*log T
2.	$a_{Ca^{+2}}/a_{H^+}^2$	$3pre + 4H^+ = 2czo + 3qtz + 2Ca^{+2} + 4H_2O$	-28.070 + 3839.34/T - 0.007605*T + 11.435*log T
3.	$a_{Fe(OH)_4^-}/a_{OH^-}$	$epi + OH^- + 2H_2O = pre + Fe(OH)_4^-$	-6.244 + 461.86/T + 0.01411*T - 2.412*log T
4.	$a_{Fe(OH)_4^-}/a_{OH^-}$	$epi + wol + OH^- + H_2O = qtz + gro + Fe(OH)_4^-$	-6.990 + 572.14/T + 0.01636*T - 2.663*log T
5.	$a_{H_2S}^3/a_{H_2}$	$2H_2 + 3\ pyr + 4H_2O = mag + 6H_2S$	0.627 - 7447.15/T + 0.008424*T + 1.282*log T
6.	a_{H_2S}/a_{H_2}	$pyr + H_2 = pyrr + H_2S$	1.938 - 1838.13/T - 0.001152*T + 0.918*log T
7.	$a_{Ca^{+2}}/a_{H^+}^2$	$2H^+ + wol = Ca^{+2} + SiO_2 + H_2O$	-2.358 + 5244.79/T -0.003416*T + 1.140*log T

Table 7. Temperature equations for the equilibrium constant for selected mineral-gas buffers. They are valid in the range 0-350°C at vapour saturation pressures and assume unit activity for all minerals, and liquid water

	Gas	Reaction	log K (T)
1	CO_2	$czo + cal + \frac{3}{2}\,qtz + H_2O = \frac{3}{2}\,pre + CO_{2\,aq}$	-1.297 –771.80/T +0.007134*T –0.310*logT
2	H_2S	$\frac{1}{3}\,pyr + \frac{1}{3}\,pyrr + \frac{2}{3}\,pre + \frac{2}{3}\,H_2O = \frac{2}{3}\,epi + H_2S_{\,aq}$	-0.481 –3129.34/T +0.005705*T +0.187*logT
3	H_2	$\frac{4}{3}\,pyrr + \frac{2}{3}\,pre + \frac{2}{3}\,H_2O = \frac{2}{3}\,epi + \frac{2}{3}\,pyr + H_{2\,aq}$	-2.411 –1296.88 /T +0.006830*T –0.725*logT
4	CO_2	$\frac{2}{5}\,czo + cal + \frac{3}{5}\,qtz = \frac{3}{5}\,gro + \frac{1}{5}\,H_2O + CO_{2\,aq}$	-26.575 –1214.93/T+0.004264*T +9.275*logT
5	H_2S	$\frac{2}{3}\,gro + \frac{1}{3}\,pyr + \frac{1}{3}\,pyrr + \frac{2}{3}\,qtz + \frac{4}{3}\,H_2O = \frac{2}{3}\,epi + \frac{2}{3}\,wol + H_2S_{\,aq}$	-0.022 –3196.99/T +0.004251*T +0.351*logT
6	H_2	$\frac{2}{3}\,gro + \frac{4}{3}\,pyrr + \frac{2}{3}\,qtz + \frac{4}{3}\,H_2O = \frac{2}{3}\,epi + \frac{2}{3}\,wol + \frac{2}{3}\,pyr + H_{2\,aq}$	-1.977 –1353.42/T +0.005440*T –0.572*logT
7	H_2S	$2gro + \frac{1}{2}\,pyr + \frac{1}{2}\,mag + 2qtz + 2H_2O = 2epi + 2wol + H_2S_{\,aq}$	1.292 –4089.69/T +0.002293*T +0.918*logT
8	H_2	$6gro + 2mag + 6qtz + 4H_2O = 6epi + 6wol + H_{2\,aq}$	3.707 –5077.06/T –0.003415*T +1.843*logT
9	H_2S	$\frac{1}{4}\,FeS2 + \frac{1}{2}\,FeS + H_2O = \frac{1}{4}\,Fe_3O_4 + H_2S_{\,aq}$	-0.691- 2746.09/T+0.005256*T+0,064*logT
10	H2	$\frac{3}{2}\,FeS + H_2O = \frac{3}{4}\,FeS_2 + \frac{1}{4}\,Fe_3O_4 + H_{2\,aq}$	-2,631- 907.34/T + 0.006412*T-0.855*logT

[a]The equations are consistent with the thermodynamic data in Table 4. The thermodynamic properties of CO_2 aq, H_2S aq and H_2 aq, were calculated with the aid of the SUPCRT 92 program (Johnson et al., 1992) using the slop98.dta data set.
The mineral phases have the following meanings; cal: calcite; czo: clinozoisite; epi: epidote; gro: grossular; ; mag: magnetite; pre: prehnite; pyr: pyrite; pyrr: pyrrhotite; qtz: quartz; wol: wollastonite.